AN ABSTRACT OF THE THESIS OF

Jacques Ronald Victor Zaneveld for the DOCTOR OF PHILOSOPHY
(Name) (Degree)

in OCEANOGRAPHY presented on May 19, 1971
(Major) (Date)

Title: OPTICAL AND HYDROGRAPHIC OBSERVATIONS OF THE CROMWELL CURRENT BETWEEN 92°00' WEST AND THE GALAPAGOS ISLANDS

Abstract approved: Redacted for Privacy
June G. Pattullo

A relation is found for the diameter of a particle as a function of depth for homogeneous waters if the particle is settling at the Stoke's velocity and is decaying at a rate related to its surface area. This relation is expanded to include vertical advection. Under these circumstances it is shown that optical parameters can be interpreted as sensitive indicators of vertical motion in the oceans.

For decaying particles it is found that the "consumption" term in the diffusion equation is equal to a function of the particle diameter multiplied by the partial derivative of the particle size distribution with respect to diameter. The function of the particle diameter is a constant in the case of decay by bacterial activity, and is inversely proportional to the particle diameter in the case of decay by mass dissolution.

The vertical diffusion equation for particle size distributions is then solved for the case of Stoke's settling and vertical advection only. A solution for the particle size distribution is also obtained when vertical mixing is included.

The region immediately West of the Galapagos Islands was investigated during February 1969. Optical and hydrographic observations were made at two meridional sections across the Cromwell current, at 92°00'W and 91°40'W longitude.

The optical features of the Cromwell current are described. Beneath the thermocline the Cromwell current is characterized by deepening of the light scattering isograms. Above the thermocline shallowing of the light scattering isograms results in a surface minimum in light scattering directly above the Cromwell current. The meridional circulation at 91°40'W as compared to that at 92°00'W has apparently been modified due to the influence of the Galapagos Islands.

In the region of the thermocline the vertical gradients of temperature, oxygen content, and light scattering are approximately one third as large at 91°40'W compared to those at 92°00'W. This reduction is attributed to increased mixing in the Cromwell current as it approaches the Galapagos Islands.

Splitting of the core of the current into a northern and less clearly indicated southern branch is inferred from the horizontal distributions of temperature, oxygen content, and light scattering just

beneath the depth of maximum horizontal velocity.

The core of the current at 91°40'W was found to be more saline, and the eastward velocity was at least three times greater than during Knauss' observations at 92°15'W in 1961, but the same as Knauss' measurements in 1959.

Another indication of the variability of the Cromwell current was found in the salinity distribution. Pockets of higher salinity water indicate the possibility of daily fluctuations in salinity of 0.25‰.

Optical and Hydrographic Observations of the Cromwell Current Between 92°00' West and the Galapagos Islands

by

Jacques Ronald Victor Zaneveld

A THESIS

submitted to

Oregon State University

in partial fulfillment of
the requirements for the
degree of

Doctor of Philosophy

June 1972

APPROVED:

Redacted for Privacy

Professor of Oceanography

in charge of major

Redacted for Privacy

Chairman of Department of Oceanography

Redacted for Privacy

Dean of Graduate School

Date thesis is presented May 19, 1971

Typed by Clover Redfern for Jacques Ronald Victor Zaneveld

ACKNOWLEDGMENTS

My sincere gratitude goes out to Dr. George F. Beardsley, Jr., whose guidance and encouragement has been of great help . His untimely death was felt as a great personal and professional loss.

Dr. June G. Pattullo graciously allowed me to complete the work under her supervision. I would like to thank her for the many suggestions and encouragement in helping me finish this work. I also thank Drs. Burt, Pond, Pak, Quinn and Paulson for reading the manuscript and for many helpful suggestions.

I am indebted to my parents without whom this work would not have been possible. The Great Turtle sees his work near completion, and can only laugh, for he has almost caught the hares--one more.

Finally I would like to thank Mr. Wasowski for help with the computer calculations and Miss Sue Wingate for moral support.

This work was supported by the Office of Naval Research contract ONR N000 14-67-A-0369-0007.

TABLE OF CONTENTS

LIST OF FIGURES

OPTICAL AND HYDROGRAPHIC OBSERVATIONS OF THE CROMWELL CURRENT BETWEEN 92°00' WEST AND THE GALAPAGOS ISLANDS

PARTICLE SIZE DISTRIBUTION AS A FUNCTION OF DEPTH IN HOMOGENEOUS WATERS AND ITS RELATION TO THE OPTICAL TRACER METHOD

Introduction

The use of light scattering and transmission properties of sea water for the identification of water masses has gained increased acceptance in recent years. The optical properties of the oceans are due to the suspended and dissolved materials and to water itself. The light scattered by a particle can be characterized by its shape and electromagnetic properties. The residence time of particles in a given watermass is usually long, as the sinking rate of the small particles is extremely slow. The optical tracer method makes use of this fact. The optical tracer method employs optical parameters for the classification of watermasses, and has been used in the past (for instance Jerlov, 1951, 1953; Joseph, 1955; Pak, Beardsley and Park, 1970).

The properties usually employed in the optical tracer method are the volume scattering function, the total scattering coefficient, and the beam extinction coefficient. These properties are defined as in Jerlov (1968). The volume scattering function is the radiant

intensity (from a volume element in a given direction) per unit of irradiance on the volume and per unit volume. The total scattering coefficient is the internal scatterance of an infinitesimally thin layer of the medium normal to the beam, divided by the thickness of the layer. The beam extinction coefficient (total attenuation coefficient) is the internal attenuance of an infinitesimally thin layer of the medium normal to the beam, divided by the thickness of the layer.

The optical parameters used are considered to be inherent properties of the water and are a function of the type and number of particles present. Light scattered by a volume element of sea water is the sum of the light scattered by the particles present in that volume and the light scattered by the water and the materials dissolved in it. The intensity and radiance pattern of the light scattered by a particle depends on its shape, size and complex index of refraction (Van De Hulst, 1957). The inherent optical properties are thus dependent on the particle size distribution (Jerlov, 1968). The inherent optical properties of sea water are not directly influenced by the external light field or daylight field. The daylight field in sea water and the image transmission qualities of sea water may be calculated however, if the inherent optical properties are known (Beardsley and Zaneveld, 1969; Zaneveld and Beardsley, 1969; Zaneveld et al., 1970). The particle size distribution is the number of particles with a given diameter present per unit volume of seawater. Mie theory can be used

to relate the particle size and index of refraction to its scattering characteristics, if the particle is assumed to be spherical and does not absorb light (Mie, 1908; Burt, 1956).

Most light scattering particles are generated or enter the ocean in the region between the ocean surface and the thermocline. These particles are detritus, dead and decaying phyto- and zooplankton, atmospheric dust, runoff from land, etc. Many of these particles have a density very close to that of seawater. The thermocline is usually accompanied by an increase in water density, and is a region of minimum turbulence (Jerlov, 1959). This explains the high light scattering usually associated with the thermocline. The thermocline is usually at the bottom of the euphotic zone. Little photosynthesis and hence particle generation takes place below the thermocline. For the layers of water beneath the thermocline, the thermocline is considered to be a source of particles.

If conditions for particle generation are uniform over a given region, so that the source for particles is horizontally uniform, large horizontal differences in the inherent optical properties can still be observed (Pak et al., 1970; Jerlov, 1951). Thus, if a horizontal maximum in light scattering is observed, sinking or mixing may be expected. Similarly, a horizontal minimum indicates upwelling or mixing. It is usually assumed that a light scattering minimum is accompanied by a lower particle concentration, and a light scattering

maximum by a particle concentration maximum. This is not necessarily so, as a change in particle size may account for a change in the inherent optical properties without changing the total particle concentration, since the intensity of light scattered depends on the size of the particle (Van De Hulst, 1957).

It is possible to detect horizontal motion by means of optical properties if a horizontal gradient of these properties exists in the first place. The optical tracer method is thus suited for the detection of vertical motion or mixing. Horizontal motion or mixing may be inferred from the horizontal displacement of maxima and minima. The optical tracer method thus is an addition to the core method, adding new variables with which to characterize a watermass.

Statement of the Problem

Previous efforts to understand the particle dynamics in the oceans have used the particle concentration as the dependent variable (Wyrtki, 1950; Riley et al., 1949; Jerlov, 1959; Ichiye, 1966a). This method of attack ignores the importance of the size distribution of the particles. This is an important omission as the optical properties of sea water are dependent not only on the concentration of particles but also on their size distribution (Pak, Zaneveld and Beardsley, 1971). In order to understand the reasons why the optical properties of sea water change, we must first understand the mechanisms by which the

particle size distributions in the ocean are altered. The problem in this section is to introduce the particle size distribution into the theoretical considerations.

Approximations Used in this Section

In order to obtain a manageable set of equations, we will make the following assumptions:

a. All particles have the same density.

b. The particles are spherical.

c. The particles decay in some way that is related to their surface area.

d. The density of the particles does not change with depth.

The first assumption is not a stringent one, as the density enters parametrically and may be changed in the final solution. The relative density of the particles involved in light scattering varies a great deal. The relative density of a particle with respect to seawater may be given by:

$$\rho' = \frac{\rho_p - \rho_w}{\rho_w} \qquad (1)$$

where ρ_p is the density of the particle and ρ_w is the density of the water. The particle size distribution may always be considered to be the sum of several particle size distributions, each with a

different density. In that case the solutions will still be valid.

The assumption of sphericity is made in order to be able to assume equal sinking rates for particles with the same diameter, and to obtain a simple expression relating the surface area to the diameter. The particles of interest are small, with a diameter less than 20 microns (Jerlov, 1968). The Stoke's settling velocity is thus a reasonable approximation.

The particles decay by means of many mechanisms, such as oxidation of organic matter, bacterial activity, dissolution of calcite shells, etc. It would be extremely difficult to include all these mechanisms explicitly into one theory. We will therefore assume that the particles decay at a rate which is related to their diameter. Bacterial activity is probably the fundamental process by which the particle size is reduced in the oceans (Jerlov, 1959). In that case it is reasonable to assume that the rate of mass loss is proportional to the surface area of the particle. In the case of mass dissolution (decay by solution) it can be shown that the rate of mass loss for particles with a diameter of less than 20 microns is proportional to the particle diameter (Pond, Pytkowicz, and Hawley, 1971).

These particles usually will change their density somewhat while they are settling, particularly if they consist of a hard inner or outer shell and protoplasm. Again, it would be difficult to include all possibilities into one theory. The assumptions made are the most

reasonable ones that still permit some mathematical manipulation.

Some particles in the ocean, such as materials of terrestrial origin do not decay at all in the oceans. The percentage of organic matter in particulate matter in sea water varies from 14% to 62% (Jerlov, 1968). Solutions for the particle size distribution as a function of depth for non-decaying particles are included in this discussion.

It is clear that any solution obtained using these rather stringent restrictions should not be considered as quantitatively useful, but should be looked upon as a first order solution indicating possible relationships between the particle size distribution and hydrographic features.

The Diameter of a Decaying Spherical Particle as a Function of Depth

We had assumed that the particle is being decayed at a rate related to its diameter. Its rate of mass loss with time is given by:

$$\frac{dM}{dt} = \frac{d}{dt}\left[\rho_p \frac{\pi a^3}{6}\right] \qquad (2)$$

where M is the total mass of the particle, and a is the diameter. Since we have assumed that the density of the particle does not change with depth, we may write:

$$\frac{dM}{dt} = \rho_p \left[\frac{d}{dt} \left(\frac{\pi a^3}{6} \right) \right] = \rho_p \frac{\pi a^2}{2} \frac{da}{dt} \tag{3}$$

or,

$$\frac{dM}{dt} = \rho_p \frac{\pi a^2}{2} R(a) \tag{4}$$

$R(a) = \frac{da}{dt}$ is a constant if the particles decay at a rate proportional to their surface area. $R(a)$ is inversely proportional to a in the case of mass dissolution. In order to maintain generality we will assume that $R(a)$ is some function of the particle diameter. We will carry the calculations as far as possible without assuming a particular form for $R(a)$.

The particles are assumed to be settling at the Stoke's velocity w_s, which is a good approximation if the Reynold's number is less than 0.5 (Prandtl and Tietjens, 1957). We will show that for the small particles under consideration the Reynold's number is always less than 0.5, so that the Stoke's approximation may be used with confidence.

The Stoke's settling velocity is given by:

$$w_s = \frac{2}{9} g \frac{a^2}{4} \frac{1}{\nu} \frac{\rho_p - \rho_w}{\rho_w} \tag{5}$$

where a is the diameter of the particle, g the acceleration due to gravity, and ν the kinematic viscosity of sea water, and $\frac{\rho_p - \rho_w}{\rho_w}$ is

the relative density term already described. Some reasonable values are:

$g = 980 \text{ cm-sec}^{-2}$

$\nu = 0.016 \text{ cm}^2\text{sec}^{-1}$ at 5° centigrade and 35‰ salinity

$\frac{\rho_p - \rho_w}{\rho_w} = 1.0$

$a = 20\mu$ at most (Jerlov, 1968).

Substituting these values into Equation 5, we see that the maximum Stoke's velocity in our case is approximately:

$$w_{smax} = 2 \times 10^{-2} \text{ cm-sec}^{-1}$$

The Reynold's number if given by:

$$Re = \frac{w_s a}{\nu} \qquad (6)$$

The largest Reynold's number to be expected is:

$$Re_{max} = 4 \times 10^{-3}$$

Since the largest Reynold's number is much less than 0.5, we can use the Stoke's approximation.

The constants in the Stoke's equation (Equation 5) can be combined to give:

$$w_s = ca^2 \tag{7}$$

where:

$$c = \frac{2}{9} g \frac{1}{4} \frac{\rho_p - \rho_w}{\nu \rho_w} \tag{8}$$

The rate of change of diameter with time was given by:

$$R(a) = \frac{da}{dt} = \frac{da}{dz}\frac{dz}{dt} = w_s \frac{da}{dz} \tag{9}$$

since $\frac{dz}{dt}$ is the settling rate given by the Stoke's velocity, w_s, we may substitute Equation 7 into 9:

$$w_s \frac{da}{dz} = ca^2 \frac{da}{dz} \tag{10}$$

so that:

$$R(a) = ca^2 \frac{da}{dz} \tag{11}$$

We now integrate from $z = z_0$ to $z = z$ where $z = z_0$ is the thermocline depth, and set $a(z) = a$; $a(z_0) = a_0$:

$$\int_{z_0}^{z} \frac{dz}{c} = \int_{a_0}^{a} \frac{a^2 da}{R(a)} \tag{12}$$

The integrals may be left in that form if we wish to consider the change of relative density and kinematic viscosity with depth, or if R is considered to be a function of a.

For a homogeneous ocean and particles decaying at a rate proportional to their surface area we may assume c constant and R independent of a. The equation may then be simplified:

$$\frac{R(z-z_0)}{c} = \frac{1}{3}(a^3 - a_0^3) \tag{13}$$

The diameter of a particle at depth z is then given by:

$$\begin{aligned} a(z) &= \left[\frac{3R}{c}(z-z_0) + a_0^3\right]^{1/3} \quad \text{for} \quad \left[\frac{3R(z-z_0)}{c} + a_0^3\right] \geq 0 \\ a(z) &= 0 \qquad\qquad\qquad\quad \text{for} \quad \left[\frac{3R(z-z_0)}{c} + a_0^3\right] < 0 \end{aligned} \tag{14}$$

Particles with diameter a_0 at z_0 decay to particles with diameter a at z. Their concentrations have not changed. The particle size distribution for that particular a and a_0 are then the same;

$$P(a, z) = P(a_0, z_0) \tag{15}$$

since a and a_0 are related as in Equation 14. We may set:

$$\begin{aligned} P(a, z) &= P\left(\left[\frac{3R}{c}(z-z_0) + a_0^3\right]^{1/3}, z_0\right) \quad \text{for} \quad \frac{3R}{c}(z-z_0) + a_0^3 \geq 0 \\ P(a, z) &= 0 \qquad\qquad\qquad\qquad\qquad\quad \text{for} \quad \frac{3R}{c}(z-z_0) + a_0^3 < 0 \end{aligned} \tag{16}$$

We have thus found a relationship between the particle size distribution at the thermocline and at any other depth. The relation shows that the average particle size decreases with depth, and that the total number of particles also decreases, as observed in nature (Jerlov, 1968; Carder, 1970).

If, besides Stoke's settling vertical advection is present, we must set:

$$w = w_s + w_0 = ca^2 + w_0 \tag{17}$$

where w_0 is the advective velocity.

Then,

$$R(a) = \frac{da}{dt} = w\frac{da}{dz} = (ca^2+w_0)\frac{da}{dz} \tag{18}$$

and proceeding as previously:

$$\int_{z_0}^{z} dz = \int_{a_0}^{a} \frac{(ca^2+w_0)da}{R(a)} \tag{19}$$

Considering R, c, and w_0 constant then gives:

$$R(z-z_0) = \frac{c}{3}(a^3-a_0^3) + w_0(a-a_0) \tag{20}$$

This result is as expected. A vertical velocity upwards is equivalent to reducing the settling rate, and therefore increasing the rate of change of diameter with depth.

Calculations were made using Equation 20 to calculate the particle size as a function of depth for various values of the vertical advection. The results are summarized in Figure 1. The particle diameter is plotted as a function of $-\frac{Rz}{c} \times 10^{-11}$, for various ratios of the vertical advective velocities w_0 and c, the Stoke's constant. Since R and c are considered to be constant throughout the water column, the ratio $-\frac{Rz}{c} \times 10^{-11}$ is proportional to the depth z. Similarly the ratio $\frac{w_0}{c}$ is proportional to the vertical advective velocity w_0. A reasonable value for c is 10^{+3} cm^{-1} sec^{-1}, so that a value of 10^{-6} for $\frac{w_0}{c}$ on the figure corresponds approximately to a vertical advective velocity of $w_0 = 10^{-3}$ cm sec^{-1}.

Some relevant conclusions may be drawn from Figure 1. The percentage of particles observed in nature larger than 20 microns is negligible (Jerlov, 1968). As an example we will consider the particles in the ocean to be of two types, non-decaying "background" particles, and decaying particles with diameters less than 20 microns. When all particles which are subject to decay with a diameter equal to or less than 20 microns have decayed entirely, the light scattering will be reduced to the scattering due to the non-decaying "background" particles. From Figure 1 we can observe that for $\frac{w_0}{c} = 0$, $-\frac{Rz}{c} = 267 \times 10^{-11}$ cm^3 when the 20 micron particles are entirely decayed. If we assume that the depth at which all decaying particles

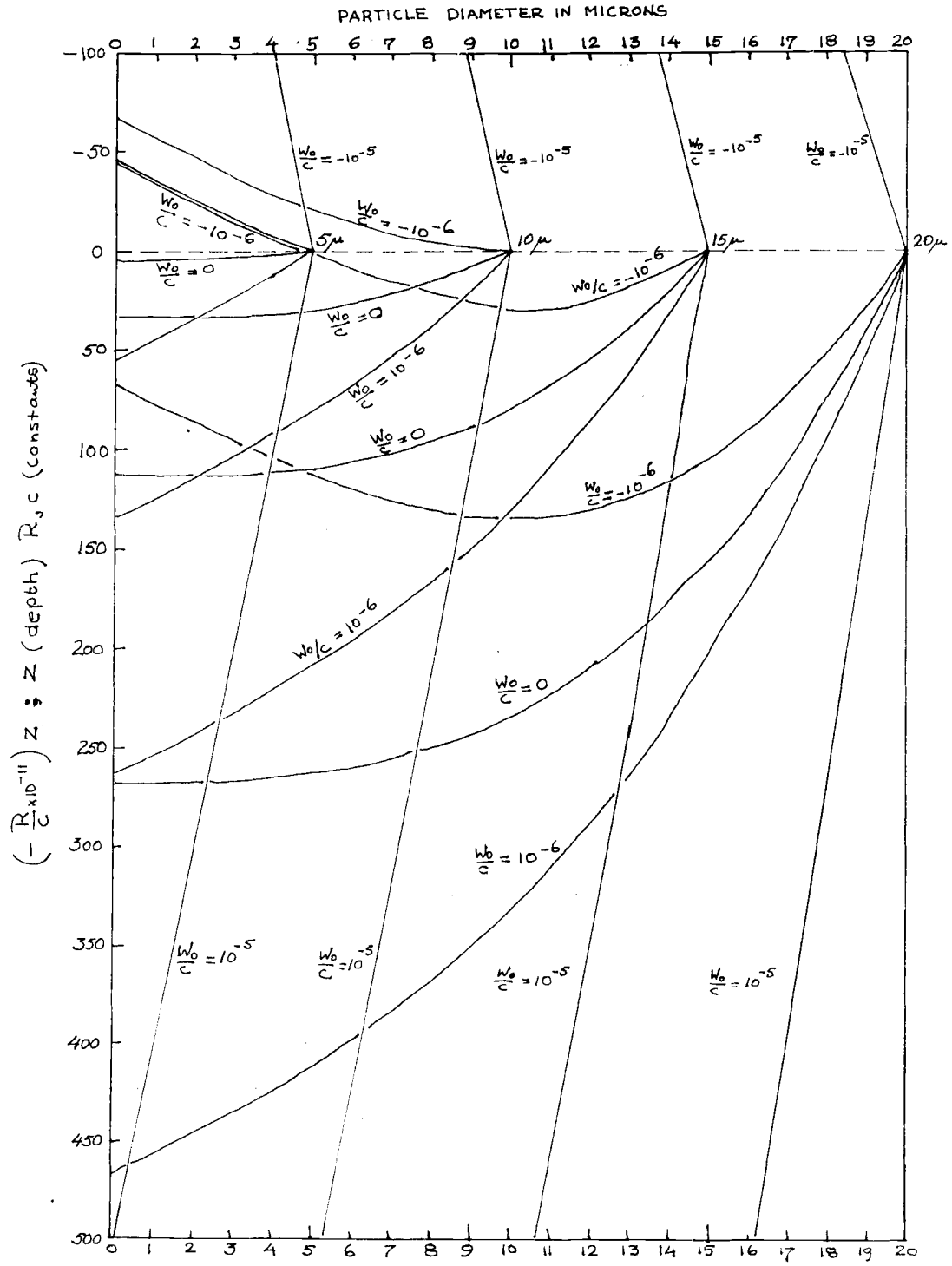

Figure 1. Particle diameter as a function of $(-\frac{R}{c} \times 10^{-11})z$ for different values of $\frac{w_0}{c}$. $(-\frac{R}{c} \times 10^{-11})z$ is proportional to depth beneath the thermocline; $\frac{w_0}{c}$ is proportional to the vertical advective velocity. The particles are settling at the Stoke's velocity and are decaying at a rate proportional to their surface area.

have disappeared is known, we may calculate a value for R. Carder (1970) indicates that below approximately 1000 m depth the particle size distribution changes very little. If we let $z = 10^5$ cm, and take $c = 10^3\ cm^{-1} sec^{-1}$, we obtain $R = -2.67 \times 10^{-11} \frac{cm}{sec}$.

For $\frac{w_0}{c} = -10^{-6}\ cm^2$, which means a vertical advective velocity upward of approximately $10^{-3} \frac{cm}{sec}$, the decaying particles would penetrate to 510 meters depth before being forced upward by vertical advection exceeding the Stoke's settling rate. If $\frac{w_0}{c} = 10^{-6}\ cm^2$, which corresponds to a downward vertical advective velocity of approximately $10^{-3} \frac{cm}{sec}$, the particles that had a diameter of 20 microns at the thermocline would penetrate to approximately 1750 m. We thus conclude that for an upward vertical advective velocity of approximately 10^{-3} cm-sec^{-1} the same value for light scattering will be observed at .51 times the depth for which no vertical advection was present. For a downward vertical advective velocity of approximately 10^{-3} cm-sec^{-1} the same light scattering will be observed at a depth 1.75 times that for when no vertical advection was present.

Figure 1 also shows that for values of $\frac{w_0}{c} \geq 10^{-5}$ the particle settling velocity is negligible compared to the vertical advective velocity. This occurs when the advective velocity is larger than $10^{-2} \frac{cm}{sec}$. Knauss (1966) estimated an average vertical velocity of approximately $10^{-3} \frac{cm}{sec}$ in the Cromwell current area. It thus

appears that even in such a turbulent area as the Cromwell current, the particle settling velocity cannot be ignored.

It should be noted that the results in Figure 1 are independent of the particle size distribution. Since the trajectories of the particles are now known, the size of each particle may be calculated at any depth. If we know the particle size distribution at any depth z_0, we may then calculate the particle size distribution at any depth z by means of Equation 12 if we know the manner in which the particles decay.

A Solution to the Vertical Diffusion Equation for the Particle Size Distribution

The particle size distribution is a non-conservative property of sea water. Particles are being generated and decayed everywhere in the oceans. If we denote the particle size distribution at (x, y, z) by $P(a, x, y, z)$, where a is the diameter, $P(a, x, y, z)$ must then satisfy the equation for non-conservative properties:

$$\frac{\partial}{\partial x}\left[A_x \frac{\partial P(a, x, y, z)}{\partial x}\right] + \frac{\partial}{\partial y}\left[A_y \frac{\partial P(a, x, y, z)}{\partial y}\right] + \frac{\partial}{\partial z}\left[A_z \frac{\partial P(a,x,y,z)}{\partial z}\right]$$

$$- \frac{\partial}{\partial x}\left[uP(a, x, y, z)\right] - \frac{\partial}{\partial y}\left[vP(a, x, y, z)\right] - \frac{\partial}{\partial z}\left[wP(a, x, y, z)\right] + G$$

$$= \frac{\partial P(a, x, y, z)}{\partial t} \qquad (21)$$

A_x, A_y, and A_z are the kinematic eddy diffusion coefficients.

u, v, and w are the x, y, and z components of the average velocity. We will take z to be positive downward. We have also neglected molecular diffusion. G is a term describing the net generation or destruction of particles at (x, y, z). We will search for a solution of Equation 21 using several assumptions.

First, we assume a stationary particle size distribution, so that $\frac{\partial P(a, x, y, z)}{\partial t} = 0$. Secondly, we assume an incompressible fluid, setting $\frac{\partial u}{\partial x} + \frac{\partial v}{\partial y} + \frac{\partial w}{\partial z} = 0$. Finally we set $\frac{\partial A_x}{\partial x}$, $\frac{\partial A_y}{\partial y}$ and $\frac{\partial A_z}{\partial z}$ equal to zero, assuming a homogeneous ocean. Under these assumptions Equation 21 reduces to:

$$A_x \frac{\partial^2 P}{\partial x^2} + A_y \frac{\partial^2 P}{\partial y^2} + A_z \frac{\partial^2 P}{\partial z^2} - u \frac{\partial P}{\partial x} - v \frac{\partial P}{\partial y} - w \frac{\partial P}{\partial z} + G = 0 \quad (22)$$

We will now take a closer look at the generation term G. We will make the same assumptions as previously. A particle can be generated only by the decay of a larger particle. The number of particles with diameter a changes in time Δt by $P(a+\Delta a, x, y, z) - P(a, x, y, z)$. A particle of diameter a is thus generated from a particle with diameter $(a+\Delta a)$ in time Δt. We then have for G:

$$G(a, x, y, z) = \frac{P(a+\Delta a, x, y, a) - P(a, x, y, z)}{\Delta t} \quad (23)$$

but,

$$R(a) = -\frac{\Delta a}{\Delta t},$$

so that

$$G(a, x, y, z) = -R(a)\,\frac{P(a+\Delta a, x, y, z) - P(a, x, y, z)}{\Delta a} \qquad (24)$$

If we now go to the limit $\Delta a \rightarrow 0$, we have:

$$G(a, x, y, z) = -R(a)\,\frac{\partial P(a, x, y, z)}{\partial a} \qquad (25)$$

Replacing G in Equation 21 gives:

$$A_x \frac{\partial^2 P}{\partial x^2} + A_y \frac{\partial^2 P}{\partial y^2} + A_z \frac{\partial^2 P}{\partial z^2} - u \frac{\partial P}{\partial x} - v \frac{\partial P}{\partial y} - w \frac{\partial P}{\partial z} = R(a) \frac{\partial P}{\partial a} \qquad (26)$$

Considering vertical motion only, we then have:

$$A_z \frac{\partial^2 P(a, z)}{\partial z^2} - w \frac{\partial P(a, z)}{\partial z} = R(a) \frac{\partial P(a, z)}{\partial a} \qquad (27)$$

Solutions to this equation are not immediately obvious as $w = w_0 + ca^2$ as before, if we cannot ignore the Stoke's settling velocity with respect to the advective velocity. We are thus faced with a nonlinear partial differential equation. We will first consider the simplest case.

We ignore the diffusion term and the advective velocity. The vertical velocity is then given by the Stoke's settling velocity only. We then have:

$$-ca^2 \frac{\partial P(a,z)}{\partial z} = R(a) \frac{\partial P(a,z)}{\partial a} \tag{28}$$

This equation is much simpler, and may be solved by separation of variables.

Let

$$P(a,z) = A(a)Z(z) \tag{29}$$

Substitute this into Equation 28:

$$-cA(a) \frac{\partial Z(z)}{\partial z} = \frac{R(a)}{a^2} Z(z) \frac{\partial A(a)}{\partial a} \tag{30}$$

or

$$-\frac{c}{Z(z)} \frac{\partial Z(z)}{\partial z} = \frac{R(a)}{a^2} \frac{1}{A(a)} \frac{\partial A(a)}{\partial a} \tag{31}$$

The left hand side is a function of z only, and the right hand side is a function of a only. Thus each side may be set equal to a separation constant, $-k_1$:

$$-c \frac{1}{Z(z)} \frac{\partial Z(z)}{\partial z} = -k_1 \tag{32}$$

And,

$$\frac{R(a)}{a^2} \frac{1}{A(a)} \frac{\partial A(a)}{\partial a} = -k_1 \tag{33}$$

Equations 32 and 33 are solved readily:

$$Z(z) = k_2 \, e^{\frac{k_1}{c} z} \tag{34}$$

$$A(a) = k_3 \, e^{-k_1 \int \frac{a^2}{R(a)} \, da} \tag{35}$$

In the case of bacterial decay of the particles $R(a)$ is constant. We then have:

$$A(a) = k_3 \, e^{-\frac{k_1}{3R} a^3} \tag{36}$$

k_1, k_2, and k_3 are constants. The particle size distribution for bacterial decay assuming no diffusion and no vertical advection is then:

$$P(a, z) = k_4 \, e^{-k_1 (\frac{a^3}{3R} - \frac{z}{c})} \tag{37}$$

k_4 and k_1 are arbitrary constants. We may sum any number of the solutions of the type in Equation 37 and still satisfy the original diffusion Equation 28. This fact can be expressed as:

$$P(a, z) = \sum_{i, j} k_{4_j} \, e^{-k_{1_i} (\frac{a^3}{3R} - \frac{z}{c})} \tag{38}$$

where we may sum over any number of constants k_{4_j} and k_{1_i}. Each exponent may be expressed as a polynomial in $-k_{1_i}(\frac{a^3}{3R} - \frac{z}{c})$. We are summing over many of these polynomials, each involving a different constant k_{1_i}. The sum in Equation 38 may thus be expressed as any arbitrary function f of $(\frac{a^3}{3R} - \frac{z}{c})$.

$$P(a, z) = f(\frac{a^3}{3R} - \frac{z}{c}) \tag{39}$$

The boundary condition $P(a, z) = P(a_0, z_0)$ may then be satisfied by choosing the arbitrary function f such that

$$P(a_0, z_0) = f(\frac{a_0^3}{3R} - \frac{z_0}{c}) \tag{40}$$

is satisfied.

We might like to include a vertical advective velocity w_0. The equation governing $P(a, z)$ then becomes:

$$-(w_0 + ca^2)\frac{\partial P(a, z)}{\partial z} = R(a)\frac{\partial P(a, z)}{\partial a} \tag{41}$$

It is readily seen that in this case $P(a, z)$ may be accommodated, taking $R(a)$ to be constant, by a solution of the form:

$$P(a, z) = k_4 + k_3 e^{-k_1(\frac{a^3}{3R} + \frac{w_0 a}{Rc} - \frac{z}{c})} \tag{42}$$

Here again k_4, k_3 and k_1 are arbitrary constants, and any number of the solutions in Equation 42 may be summed to satisfy Equation 41. The general solution to Equation 41 is thus:

$$P(a, z) = f(\frac{a^3}{3R} + \frac{w_0 a}{Rc} - \frac{z}{c}) \tag{43}$$

Where f is any arbitrary function.

We may satisfy the boundary condition as previously. At the thermocline $a = a_0$ and $z = z_0$. The number of particles with diameter a at z is the same as the number of particles from which they decayed with diameter a_0 at z_0. We may thus take their particle size distributions to be equal:

$$k_4 + f(\frac{a_0^3}{3R} + \frac{w_0 a_0}{Rc} - \frac{z_0}{c}) = k_4 + f(\frac{a^3}{3R} + \frac{w_0 a}{Rc} - \frac{z}{c}) \tag{44}$$

so that if f is single valued we may set:

$$(a_0^3 - a^3)\frac{c}{3} + w_0(a - a_0) = R(z - z_0) \tag{45}$$

Equation 45 is the same as Equation 20 which was obtained for the diameter of a single decaying particle as a function of depth.

Returning to Equation 27, we might want to include the vertical mixing term. The equation governing the particle size distribution then becomes:

$$A_z \frac{\partial^2 P(a,z)}{\partial z^2} - (w_0 + ca^2) \frac{\partial P(a,z)}{\partial z} = R(a) \frac{\partial P(a,z)}{\partial a} \qquad (46)$$

We assume a solution of the form:

$$P(a,z) = k_4 + e^{g(a) + k_1 z} \qquad (47)$$

where $g(a)$ is to be determined. Substituting Equation 47 into Equation 46, we have:

$$A_z k_1^2 - (w_0 + ca^2) k_1 = R(a) g'(a) \qquad (48)$$

or

$$g(a) = \int \frac{1}{R(a)} [A_z k_1^2 - (w_0 + ca^2) k_1] da + \ln k_3 \qquad (49)$$

with $R(a)$ constant, Equation 49 reduces to

$$g(a) = \frac{1}{R} [A_z k_1^2 a - k_1 (w_0 a + \frac{ca^3}{3})] + \ln k_3 \qquad (50$$

We thus have for $P(a,z)$:

$$P(a,z) = k_4 + k_3 e^{\frac{A_z}{R} a k_1^2 + \frac{k_1}{R} (Rz - w_0 a - \frac{ca^3}{3})} \qquad (51)$$

Again we may sum over any number of arbitrary constants k_1 and k_3. $P(a,z)$ can then be expressed as:

$$P(a, z) = k_4 + \sum_j k_{3_j} e^{\frac{A_z}{R} a k_{1_i}^2 + \frac{k_{1_i}}{R} (Rz - w_0 a - \frac{ca^3}{3})} \tag{52}$$

Equation 52 can be expressed as any arbitrary function in a if the depth z is given. The variable in the arbitrary function is not obvious due to the presence of the $k_{1_i}^2$ terms. It is possible to express the sum in Equation 52 as

$$P(a, z) = k_4 + f\left(\frac{Rz - w_0 a - \frac{ca^3}{3}}{R}\right) f^*\left(\frac{A_z}{R} a\right) \tag{53}$$

where f is any arbitrary function obtained by defining the k_{1_i}. f^* is then also defined. Equation 53 permits us to take any particle size distribution at any depth and to derive the particle size distribution at any depth below the first, provided c, R, A_z and w_0 are given.

In the case of non-decaying particles $R(a) = 0$. The equation for $P(a, z)$ is then given by:

$$A_z \frac{\partial^2 P(a, z)}{\partial z^2} - (w_0 + ca^2) \frac{\partial P(a, z)}{\partial z} = 0 \tag{54}$$

A solution to this equation is:

$$P(a,z) = k_1(a) + k_2(a)\, e^{-\frac{w_0 + ca^2}{A_z} z} \qquad (55)$$

where $k_1(a)$ and $k_2(a)$ are arbitrary functions of a.

Discussion

The diameter of a particle settling at the Stoke's velocity as a function of depth was obtained using a variety of assumptions. The most stringent assumptions are that the density of an individual particle does not change as it settles, and that the particles have a decay rate proportional to their surface area. No good data are available to test the degree of error in each of the assumptions. The use of both of the assumptions must lead one to the conclusion that any solution is a first order one and only qualitatively correct. The solution is significant however in that it illustrates the usefulness of optical parameters as tracers of vertical motion in the ocean.

At the present there is scarcely any data for the particle size distribution as a function of depth. Carder (1970) reports some measurements but the depth spacing is much too large for the data to be suitable for the testing of the theory. New instrumentation is being developed by the Oregon State University optical oceanography group for the rapid determination of particle size distributions as a function of depth. In the near future this instrumentation will permit the

testing of the theories presented.

Since the theory permits any particle size distribution as the boundary condition, the depth dependency must provide the real test for the theory. Carder (1970) states that an exponential particle size distribution is a close approximation to the distributions which he has observed. If the particle size distribution is exponential then the depth dependence must also be exponential (Equation 51). Wyrtki (1962) has used an experimentally obtained exponential distribution with depth of oxidizable material to explain the oxygen minimum in the oceans. This depth dependence provides at least a qualitative test of the theory.

Qualitatively, the theory permits one to draw the following conclusions. High vertical particle gradients tend to develop whenever the vertical eddy diffusion is minimal, and low vertical particle gradients can be expected when the eddy diffusion reaches a maximum. Upward vertical advection increases the vertical gradient of particle concentrations, and downward advection decreases the vertical gradient of particle concentrations. An increase in relative density of the particle with respect to sea water increases the downward velocity and hence decreases the vertical gradient of particle concentrations. A decrease in relative density increases the vertical gradient of particle concentrations. These effects can occur simultaneously and could cancel each other or enhance each other.

OPTICAL AND HYDROGRAPHIC PROPERTIES OF THE CROMWELL CURRENT BETWEEN 92°00' WEST AND THE GALAPAGOS ISLANDS

Introduction

The Equatorial Undercurrent in the Atlantic Ocean was first described by Buchanan in 1886 (Buchanan, 1886, 1888). This major feature of the ocean circulation was subsequently forgotten. It was rediscovered in the Pacific Ocean in 1952 by Townsend Cromwell (Cromwell et al., 1954). Since 1954 the Equatorial Undercurrent has received a great deal of attention. Experimental programs have been carried out in the Atlantic, Pacific and Indian oceans. The Equatorial Undercurrent appears to be a permanent feature in the Atlantic and Pacific Oceans (Neumann, 1969; Montgomery, 1962) and appears at the end of the Northeast monsoon in the Indian Ocean (Swallow, 1964; Taft, 1967).

The general features of the Equatorial Undercurrent in the Pacific Ocean (Cromwell current) are well known and are adequately described elsewhere (Knauss, 1960; Montgomery, 1962; Knauss, 1966), so that a brief description here will suffice.

The Cromwell current has been observed at least as far West as 142°E longitude (Hisard et al., 1969), and as far East as the South American continent (White, 1969). The current is confined to two

degrees latitude on either side of the equator, and is approximately 200 meters thick. The depth of maximum eastward velocity slopes upwards to the East over to about 93°W, and closely follows the thermocline. Velocities larger than 150 cm-sec^{-1} have been observed. Velocities greater than 100 cm-sec^{-1} are present as far East as 95° West.

Many theoretical papers have appeared on the subject of the Equatorial Undercurrents, (for instance Charney, 1960; Robinson, 1960, 1966; Long, 1961; Wyrtki and Bennet, 1963; Ichiye, 1964) but many of the features are still unexplained.

The Galapagos Islands straddle the Equator. The islands Isla Fernandina and Isla Isabela form the Western edge of the Galapagos archipelago. Their western boundary lies at approximately 91°30'W, between 0°10'N and 1°04'S latitude. These islands greatly modify the flow of the Cromwell current. The Cromwell current is believed to normally split into a northern and southern branch (Knauss, 1966; Yoshida, 1967; White, 1969). The southern branch is presumable much weaker than the northern branch and could not be measured using a current meter (Knauss, 1966).

As indicated by Knauss' (1966) current meter measurements in 1961, the depth of maximum eastward velocity is 70 meters at 93°24'W, increases to 120 meters at 92°16'W, and descends to 200 meters at 84°00'W. The speed in the core of the current is reduced

from 65 cm-sec^{-1} at 93°24'W to 15 cm-sec^{-1} at 92°16'W and 22 cm-sec^{-1} at 87°00'West. The Galapagos area thus is interesting in that is causes large changes in a major ocean current in a relatively short distance. The mechanisms of the modifications are as yet little understood.

Statement of Problems

The Cromwell current can be identified by means of the distributions of the hydrographic properties temperature, salinity, and oxygen content. One problem to which an answer was sought during Yaloc'69 was the possibility of the existence of typical distributions of optical properties by which the waters of the Cromwell current might be identified.

As has been indicated in Section I, optical properties are particularly well suited for the identification of vertical motion in the ocean. The measurement of optical properties might, when combined with the usual hydrographic properties, give new insight into the meridional circulation in the Cromwell current regime, and its modification due to the Galapagos Islands.

The area immediately West of the Galapagos islands should be an area of increased turbulence, as much of the kinetic energy of the current is dissipated in the region. Evidence of increased mixing was thus being looked for in the experimental program.

The splitting of the Cromwell current occurs in the area of investigation. A test of the optical tracer method was performed by investigating its ability to indicate the splitting of the current. The distribution of the hydrographic properties might confirm the splitting of the current immediately West of the islands rather than further upstream.

Experimental Program

During February 1969 the Cromwell current was traversed by two North-South series of hydrographic stations along 92°00'W and 91°40'W longitude (Figure 2). Since the western edge of the Galapagos archipelago lies at approximately 91°30'W, the two series of hydrographic stations were thus taken at approximately 30 and 10 nautical miles from the western boundary of the islands. The section at 92°00'W consists of eight hydrostations and the section at 91°40'W consists of fourteen stations. At each station a hydrocast was taken and temperature, salinity and oxygen content were measured as well as light scattering at 45° from the forward and particle content for particles with a diameter greater than 2.2 microns. Light scattering at 45° from the forward direction for light with a wavelength of 546 mμ was determined in the ship's laboratory by examining water samples with a Brice-Phoenix light scattering photometer. The operation and calibration of this instrument have been described in

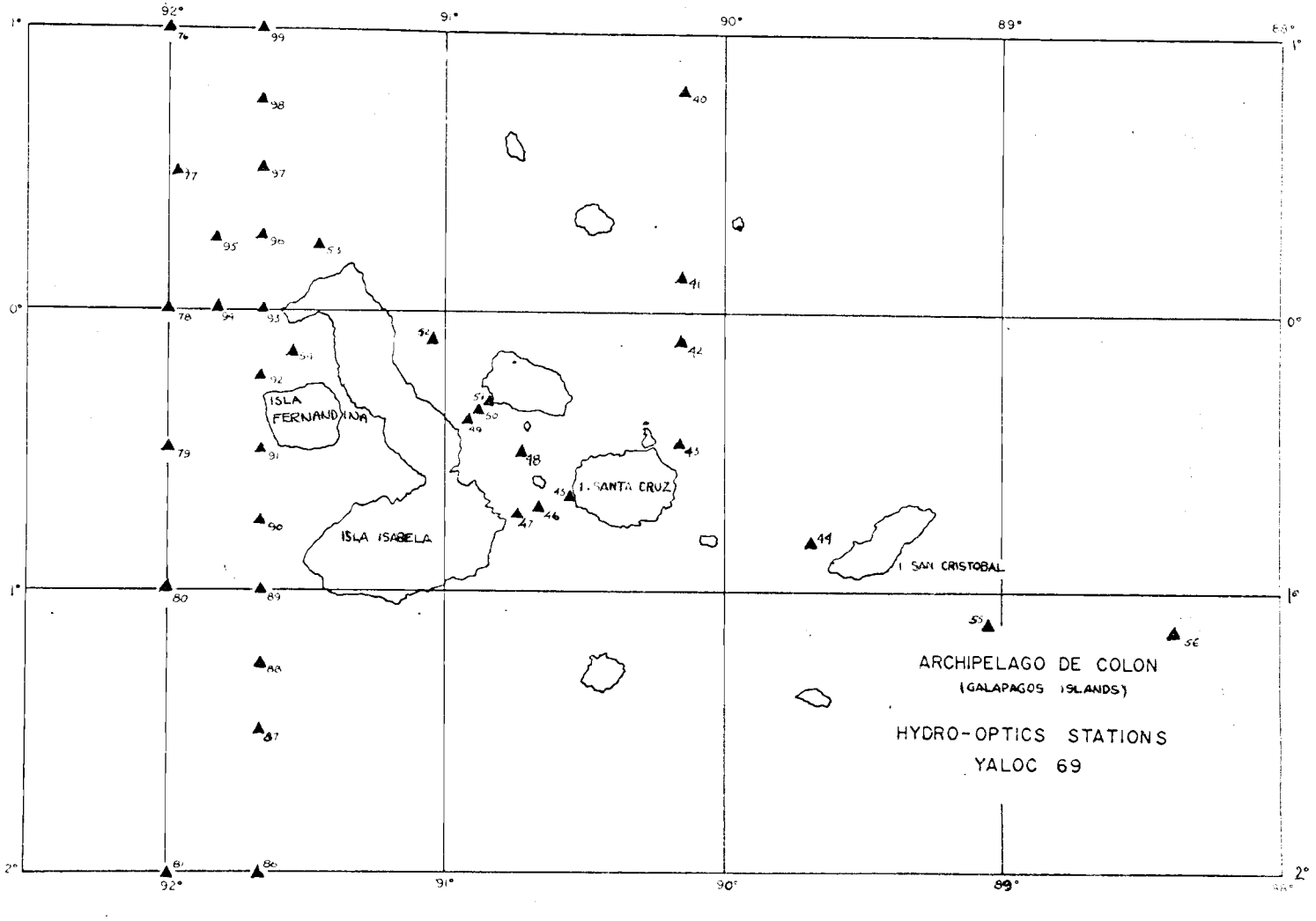

Figure 2. Stations around the Galapagos Islands.

detail by Pak (1969). The particle count for particles with a diameter greater than 2.2 microns and smaller than 50 microns was determined by means of a Coulter counter. This instrument has been described by Carder (1970). Bathythermograph and light transmissometer casts were also taken to check the results of the hydrocasts. One parachute drogue was released at the equator 10 miles West of Isla Isabela.

Graphs of the meridional distributions of salinity, temperature, oxygen content, density, light scattering and particle content were made for the sections at 92°00'W and 91°40'W. The horizontal distributions of these variables were plotted for depths of 0, 100, and 200 meters. Some of these graphs are referred to in the text and are included there. The graphs not used in the text are shown in the Appendix.

Hydrographic Observations of the Cromwell Current at 92°00'W

The presence of the Cromwell current can be inferred from the temperature structure near the equator. The presence of the Cromwell current is indicated by deepening of isothermal surfaces beneath the thermocline and to a lesser extent by shallowing of the isothermal surfaces above the thermocline. This feature was first associated with the Cromwell current by Wooster and Jennings (1955) and Wooster and Cromwell (1958).

Figure 3 shows the temperature structure as observed at

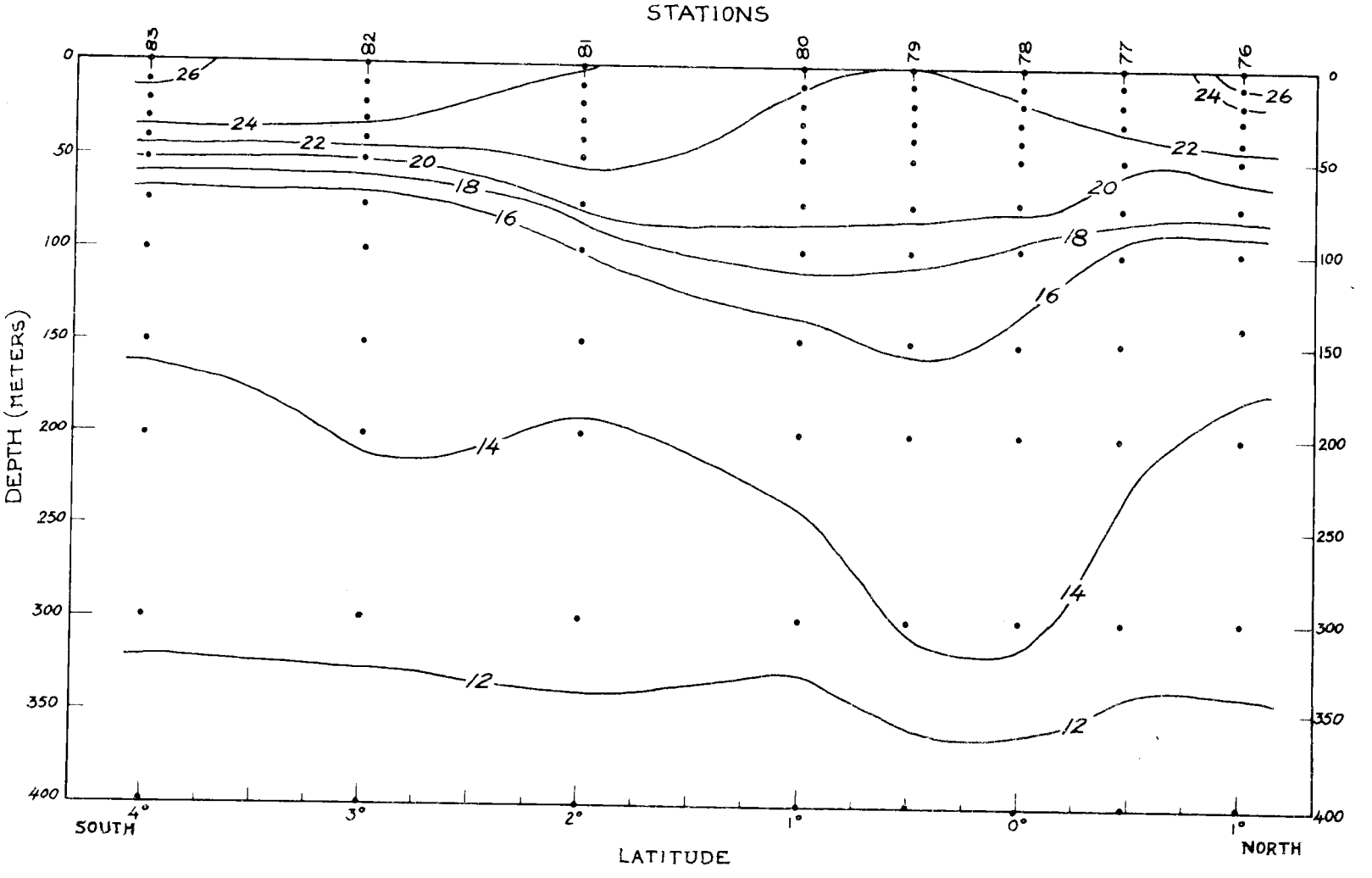

Figure 3. Temperature (°C) at 92°00'W longitude.

92°00'W during February 1969. A strong thermocline exists clearly to the South of 3°S at approximately 50 m depth. A slightly weaker thermocline is apparent to the North of 1°N, also at 50 m depth. The most nearly level isotherm in the Cromwell current region is the 20°C isotherm at approximately 60 m depth. Between 2°S and 1°N the thermocline is weakened considerably. Deepening of the isotherms occurred between 3°S and 1°N latitude between 50 m and 350 m depth. The depth of the 16°C isotherm at 3°00 S is 75 m, and at 0°30'S the depth is 160 m. The 14°C isotherm descends from 220 m at 3°00'S to 320 m at 0°15'S. Above 50 m between 2°00'S and 1°00'N shallowing of the isotherms was observed.

Several isotherms intersect the sea surface. At 4°00'S the surface temperature is greater than 26°C. At 2°00'S the surface temperature is 24°C, and at 0°30'S the surface temperature is only 22°C. This North-South gradient in temperature at the surface is greater than 1°C per degree latitude. The 22°C isotherm ascends from 40 m depth at 3°00'S to the surface at 0°30'S.

Forrester (1964) examined 47 temperature sections across the equator, and found the isotherm spreading to be least developed during the months of January and February at 140°W to 150°W. At 140°W to 150°W his maximum vertical separation of the 25°C and 15°C isotherms, averaged over six observations, is 90 m. Thus the minimum vertical temperature gradient was .11°C/m. Our observations

indicate a maximum separation for the 24°C and 16°C isotherms of 160 m. This gives a minimum vertical temperature gradient of 0.05°C/m. During February 1969 at 92°00'W the vertical temperature gradient was more than twice as small as the yearly average at 140°W-150°W. We may thus conclude that, since the spreading of the isotherms was present, and the minimum temperature gradient was less than the yearly average upstream, the Cromwell current was present and well-developed during February 1969 at 92°00'W.

In the Atlantic Ocean the Equatorial Undercurrent is associated with a salinity maximum (Metcalf, Voorhis and Stalcup, 1962). In the Pacific Ocean a tongue of high salinity water extends from the South into the Cromwell current at a depth of approximately 100 meters (Knauss, 1966). This feature was observed during Yaloc'69 (Figure 4).

Beneath the high velocity core the Cromwell current region is characterized by extremely small vertical oxygen content gradients of less than 0.01 ml/l/m (Bennett, 1963). We observed a similar feature at 92°00'W (Figure 5). The minimum vertical oxygen content gradient we observed occurred between 0°30'S and 0°15'N, and between 100 m and 300 m depth. This area has an almost uniform oxygen content between 3.00 ml/l and 2.75 ml/l. The vertical oxygen content gradient in this area is less than 0.002 ml/l/m.

Our observed hydrographic properties at 92°00'W thus resemble

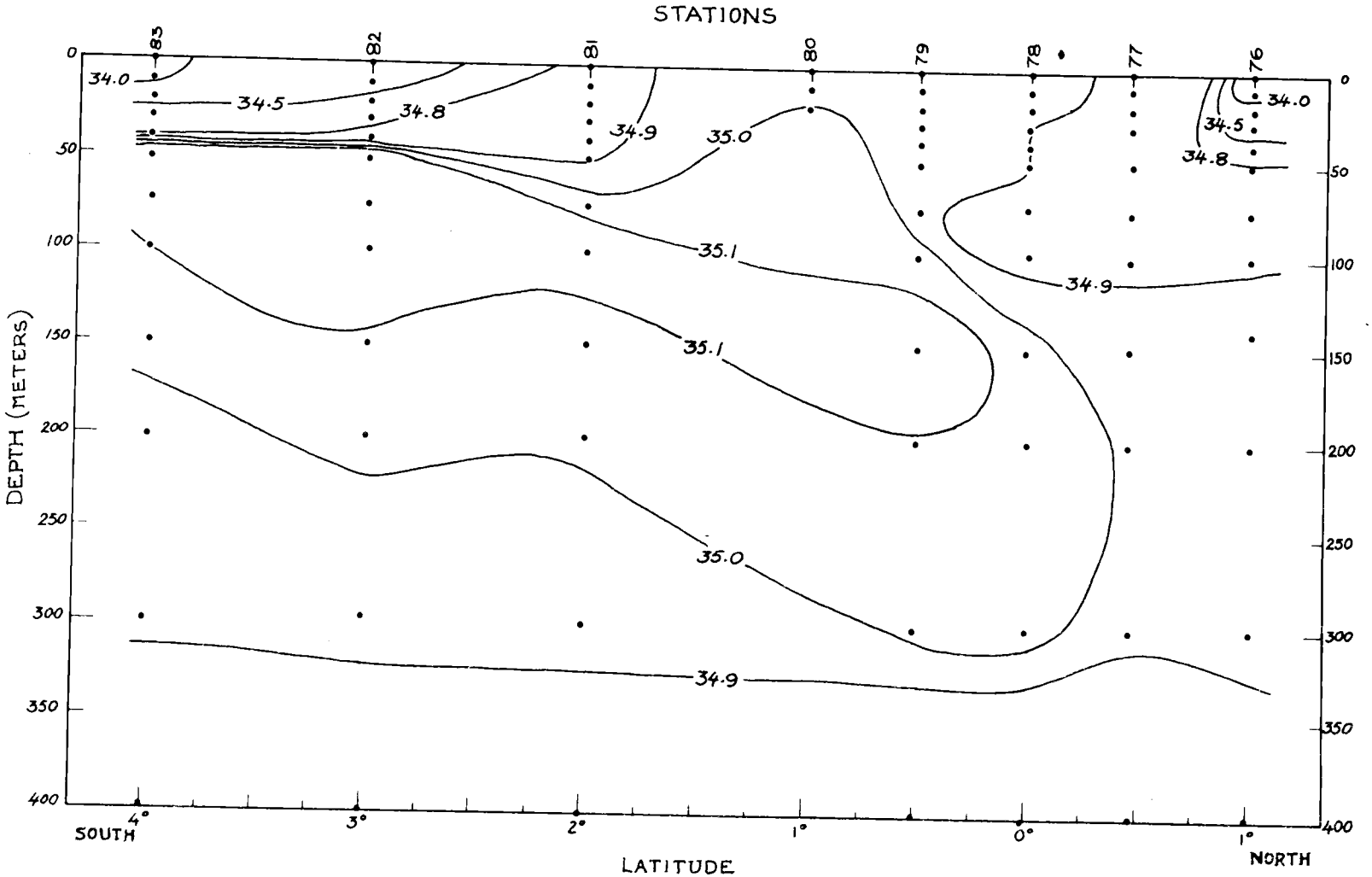

Figure 4. Salinity (‰) at 92°00'W longitude.

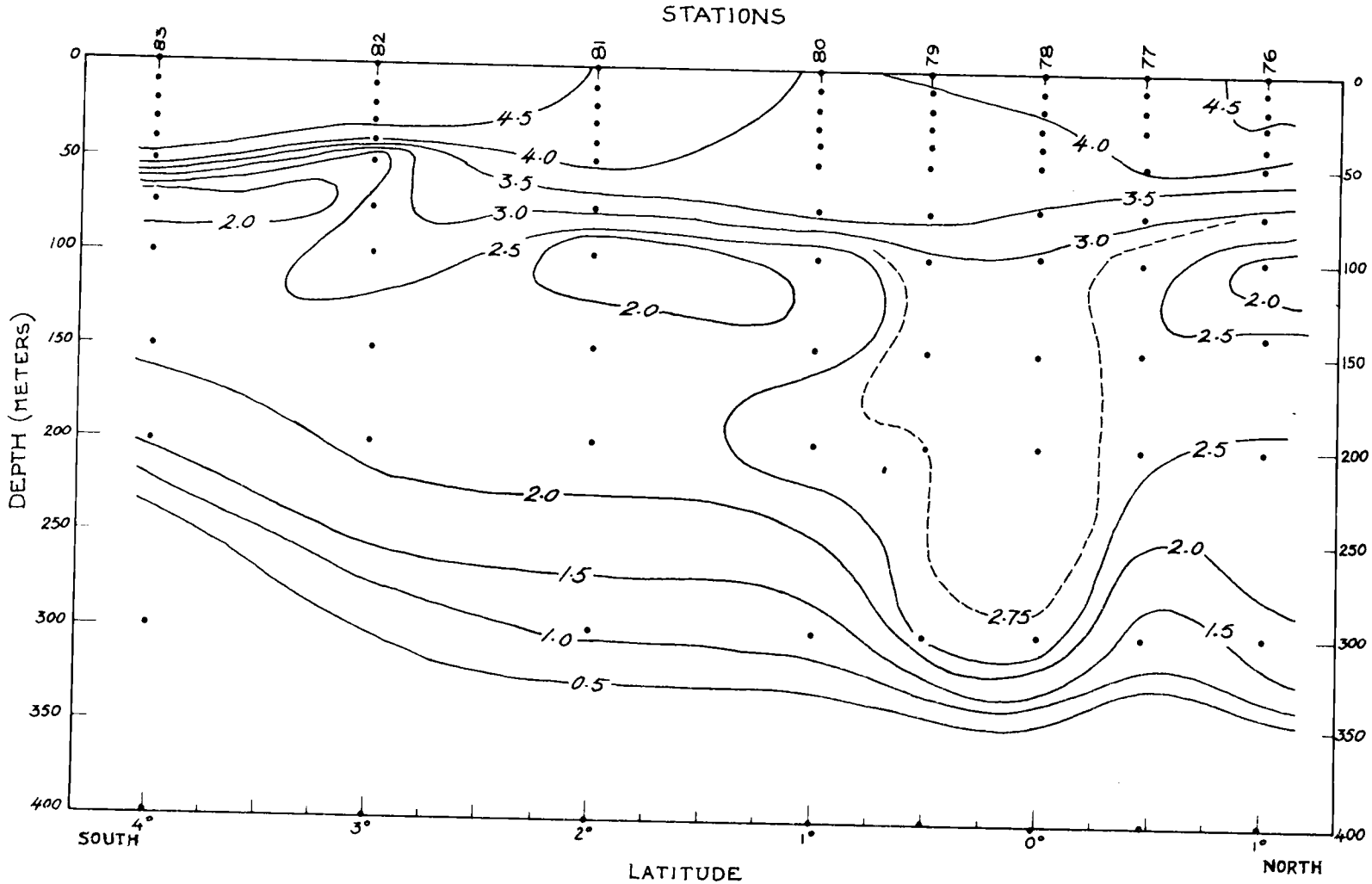

Figure 5. Oxygen content (ml/l) at 92° 00'W longitude.

those further upstream. The vertical gradients of the hydrographic properties in the Cromwell current were much smaller than the yearly averages upstream. As will be described in a later section, this feature is even more pronounced at 91°40'W. The decreased vertical gradients are ascribed to increased mixing closer to the Galapagos islands, and will be discussed later.

Optical Properties of the Cromwell Current

In the previous section we showed that the hydrographic properties at 92°00'W indicated that the Cromwell current was present. Since the Cromwell current is characterized by typical hydrographic properties, such as spreading of iosgrams, it seems likely that the Cromwell current would exhibit its own typical light scattering distributions, and its own typical particle count distributions. From our observations during Yaloc'69 we will now give a description of the optical properties of the Cromwell current.

Figure 6 shows the distribution of light scattering at 45° from the forward direction, $\beta(45)$, for the meridional section at 92°00'W. The distribution of light scattering in the Cromwell current is in many ways similar to the distribution of the hydrographic properties.

Figure 6 shows that at 1°00'N latitude and at 3°00'S latitude there are well-developed vertical gradients of light scattering

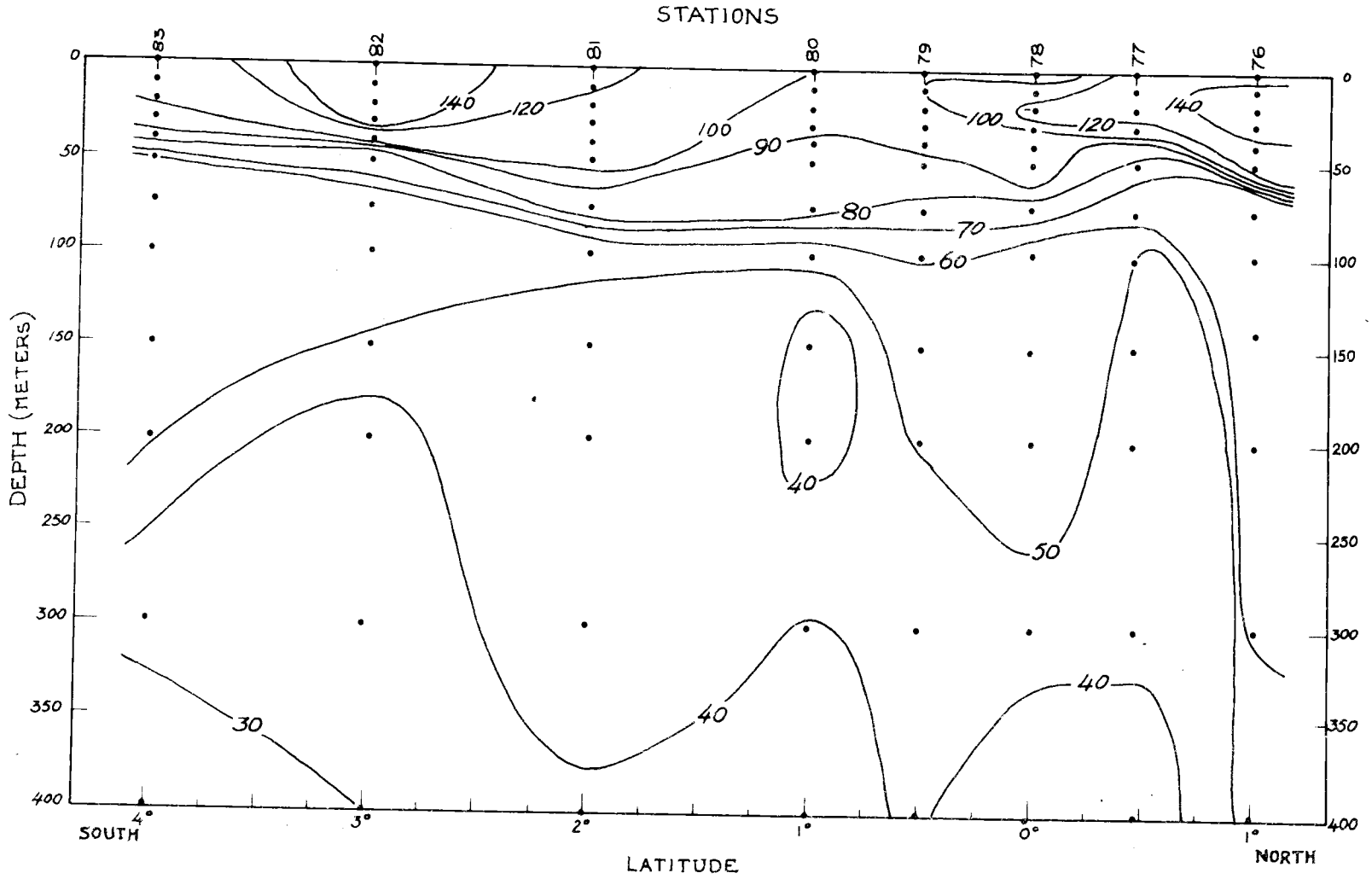

Figure 6. Light scattering at 45° $(\text{m-steradian})^{-1} \times 10^{-4}$ at 92°00'W longitude.

associated with the thermocline at approximately 50 m depth. At 3°00'S the vertical light scattering gradient at 50 m depth is approximately 2×10^{-4} (m-ster.)$^{-1}$/m, and at 1°00'N the vertical gradient at 60 m depth is approximately 3×10^{-4} (m-ster.)$^{-1}$/m. The vertical light scattering gradient in the thermocline is weakened between 0°30'N and 2°00'S latitudes. At 0°00' the vertical light scattering gradient at 50 m is 0.4×10^{-4} (m-ster.)$^{-1}$/m, and at the same depth at 2°00'S the gradient is 1.0×10^{-4} (m-ster.)$^{-1}$/m.

As we have shown the thermocline exists to the North and South of the Cromwell current, but the temperature gradient is weakened in the Cromwell current. The same is true for light scattering. The mechanism that maintains the high scattering gradient near 50 m depth to the North and South of the Cromwell current is probably the same as the mechanism maintaining the thermocline itself. The thermocline is a region of minimal vertical eddy diffusion as the stability is large (Jerlov, 1959). As was shown in the theoretical section a minimum in eddy diffusion can be related to high scattering gradient. The high light scattering gradients to the South of 3°S and to the North of 1°N at approximately 50 m depth in the region of the thermocline can thus be accounted for.

In the surface layer between 0 m and 50 m depth small light scattering gradients can be observed. The surface layer is well-mixed so that the theory predicts low light scattering gradients.

A related feature is a meridional surface minimum in $\beta(45)$ above the Cromwell current. This observation must be compared with those of Jerlov taken during the Swedish Deep-Sea expedition. Jerlov (1953) describes a particle concentration maximum between 2°N and 2°S latitude. Jerlov's surface maximum in particle concentration may be explained by increased plankton activity due to upwelling water that is rich in nutrients. We observed a narrow minimum in light scattering above the Cromwell current between 1°S and 0° latitude. The narrow minimum we observed is embedded in the broader maximum observed by Jerlov and ourselves. The region of minimum light scattering at the surface must be attributed to mixing or upwelling of the deeper and clearer water. Once at the surface this water is carried away from the equator, and induces increased plankton growth as it is rich in nutrients.

Observations of particle counts typically show greater variability than light scattering measurements and hence do not show the same detail. The only feature clearly present is the deepening of the particle concentration isograms beneath 50 m depth in the region between 0°30'N and 1°00'S latitudes (Figure 7).

Meridional Circulation

Several attempts have been made to calculate meridional circulation features theoretically (Charney, 1960; Hidaka, 1966; Ichiye,

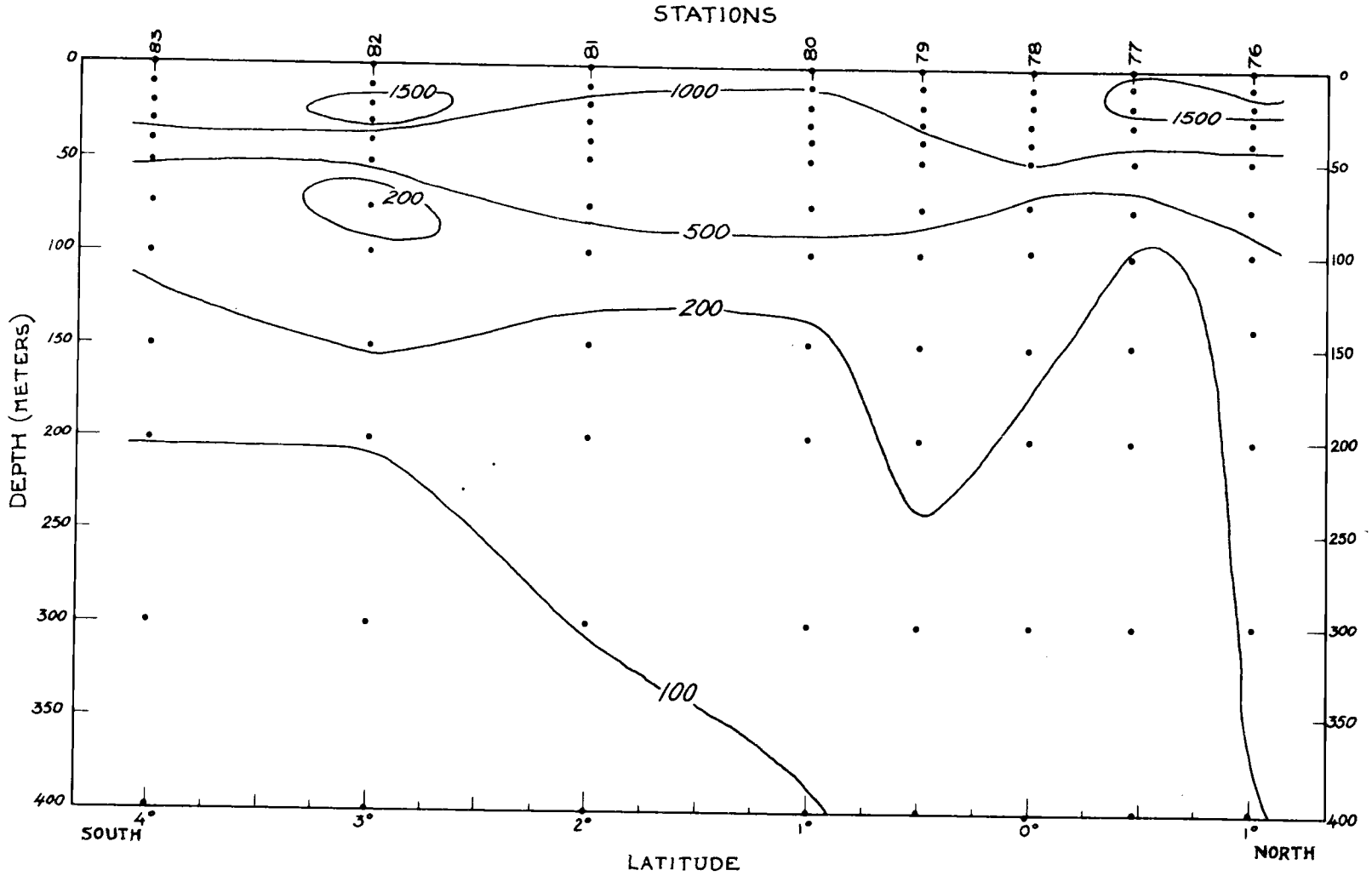

Figure 7. Total particle content per cc for particles with diameters greater than 2.2μ at 92°00'W.

1966b; Takano, 1967). The results are not conclusive, and are difficult to verify. Direct measurements using current meters (Knauss, 1966) are difficult to interpret as the ratios of zonal to meridional velocities are high. Knauss (1966) summarizes the meridional circulation as inferred from the distribution of hydrographic properties and current meter observations. Water is entrained into the Cromwell current from both sides. This entrainment results in an equatorward flow at the depth of the Cromwell current. There is evidence for this flow in the salinity distributions in the Atlantic and Pacific Oceans. In the Pacific Ocean there is a tongue of high salinity water extending from the South to the equator. In the Atlantic there are two such tongues, one from the North and one from the South. The Pacific tongue of high salinity water extending from the South is clearly visible in our data. In the high-velocity core of the Cromwell current the water is then mixed or advected upwards above the depth of the thermocline, and mixed or advected downwards beneath the thermocline. There is ample evidence for equatorial upwelling or mixing with deeper waters. There is increased productivity at the equator as has already been described. Surface minima in temperature and oxygen content directly above the Cromwell current have long been observed at the equator (for instance Bennett, 1963).

Our observations at 92°00'W add some new insight into the meridional circulation pattern. They are in general agreement with

the pattern described above. To illustrate the mixing and advection pattern the local maxima and minima of the various observed variables were examined (Figure 8). Each line on Figure 8 corresponds to the center of a tongue of water with either higher values of a property than the surrounding water (maxima or ridges) or lower values than the surrounding water (minima or troughs). We can obtain information concerning advection or diffusion by seeing how many of the maxima or minima lie in a region. If many maxima occur in a particular region, we may assume downward advection or diffusion of water, as the shallower water generally has higher temperatures, oxygen content, and light scattering. Similarly, if many minima occur in a region, upwelling or upward diffusion is expected. The salinity distribution in the Cromwell current area shows a maximum between 150 and 200 m depths, so that a salinity maximum above these depths indicates upward motion, whereas a salinity maximum below those depths indicates downward motion.

Figure 8 shows the troughs and ridges in the distribution of the several observed variables. One can see the upward mixing or advection above the thermocline (50 m) between 1°30'S and 0°00' as shown by the shallowing of the isograms of $\beta(45)$, temperature, and oxygen content. The downward mixing or advection beneath 150 meters between 0°15'N and 1°00'S is more apparent; here horizontal maxima occur in the distributions of all observed variables.

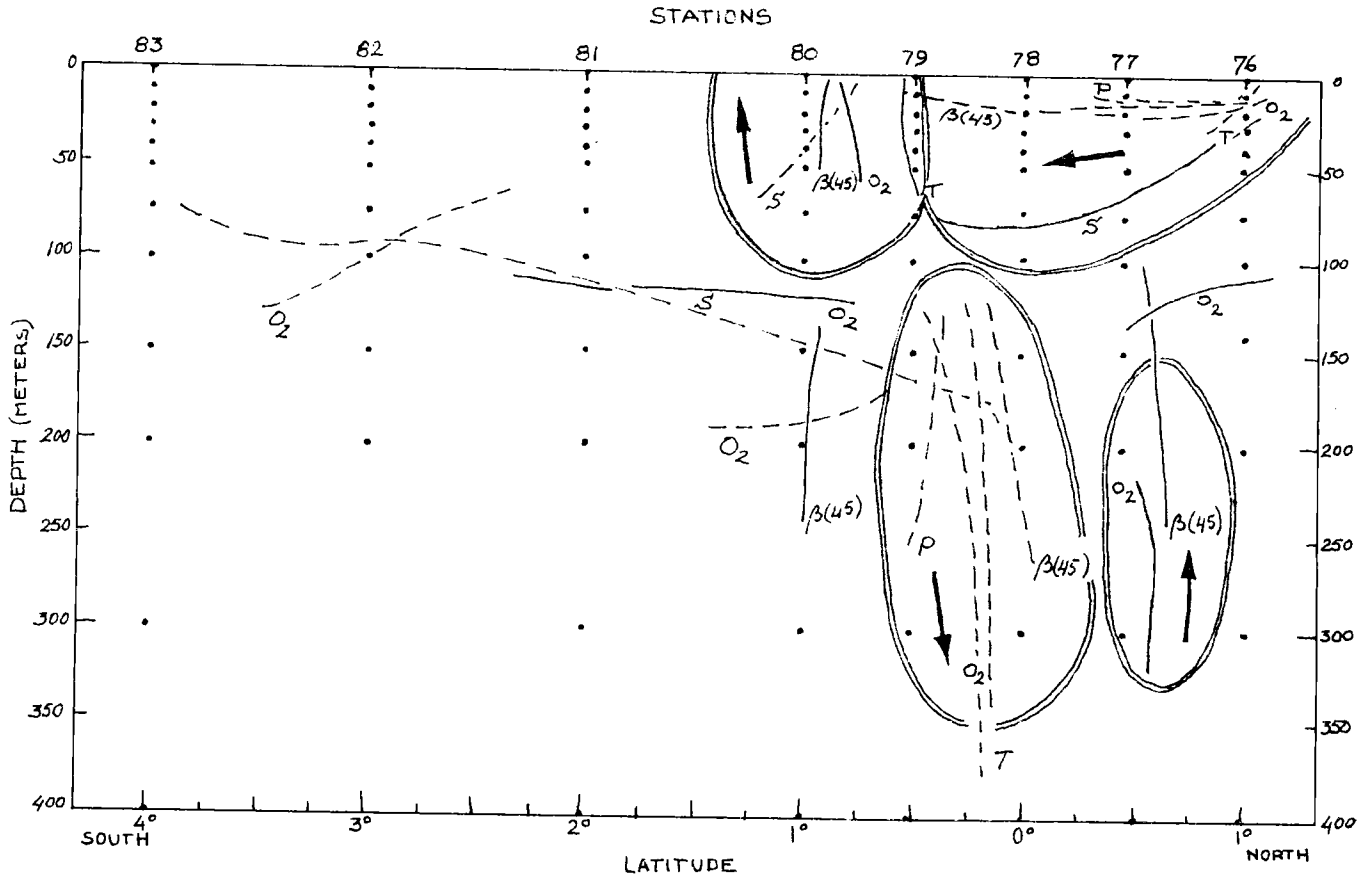

Figure 8. Local maxima (ridges) and minima (troughs) in the distributions of salinity (S), temperature (T), oxygen content (O_2), light scattering ($\beta(45)$), and total particle content (P), at 92°00' West. Maxima are indicated by dashed lines; minima by solid lines. Double lines enclose areas where advection or mixing is suggested. Arrows indicate average direction of maxima or minima.

At 1°00'N an equatorial front was observed (Zaneveld et al., 1969). Mixing of the water to the North of the front with that to the South of the front is suggested by the maxima in temperature, oxygen content and light scattering, and a minimum in salinity extending from the front.

There is some evidence of upwelling water at approximately 0°30'N between 150 and 300 m depth, indicated by local minima in $\beta(45)$ and oxygen content. The evidence is inconclusive as the minima are rather weak. The Eastropac data (Bennett, 1963) shows similar horizontal minima in the oxygen content at approximately 1°00'N. Upwelling water at approximately 1°00'N as indicated by light scattering and oxygen content may be a permanent feature of the meridional circulation in the Cromwell current.

At 91°40'W the local maxima and minima of the various observed properties present a different pattern (Figure 9) as compared with those at 92°00'W. At 91°40'W the local maxima and minima of the variables lie much closer together. A major change with respect to 92°00'W are the more prominent regions of upwelling and sinking. Between 0°00' and 0°30N there is an upwelling area between the surface and 100 m depth. A sinking region exists below 50 m between 0°45'S and 0°15'S latitude. Also apparent is a region in which the water at the surface located near 1°00'N mixes with water to the South. This region is the equatorial front mentioned earlier.

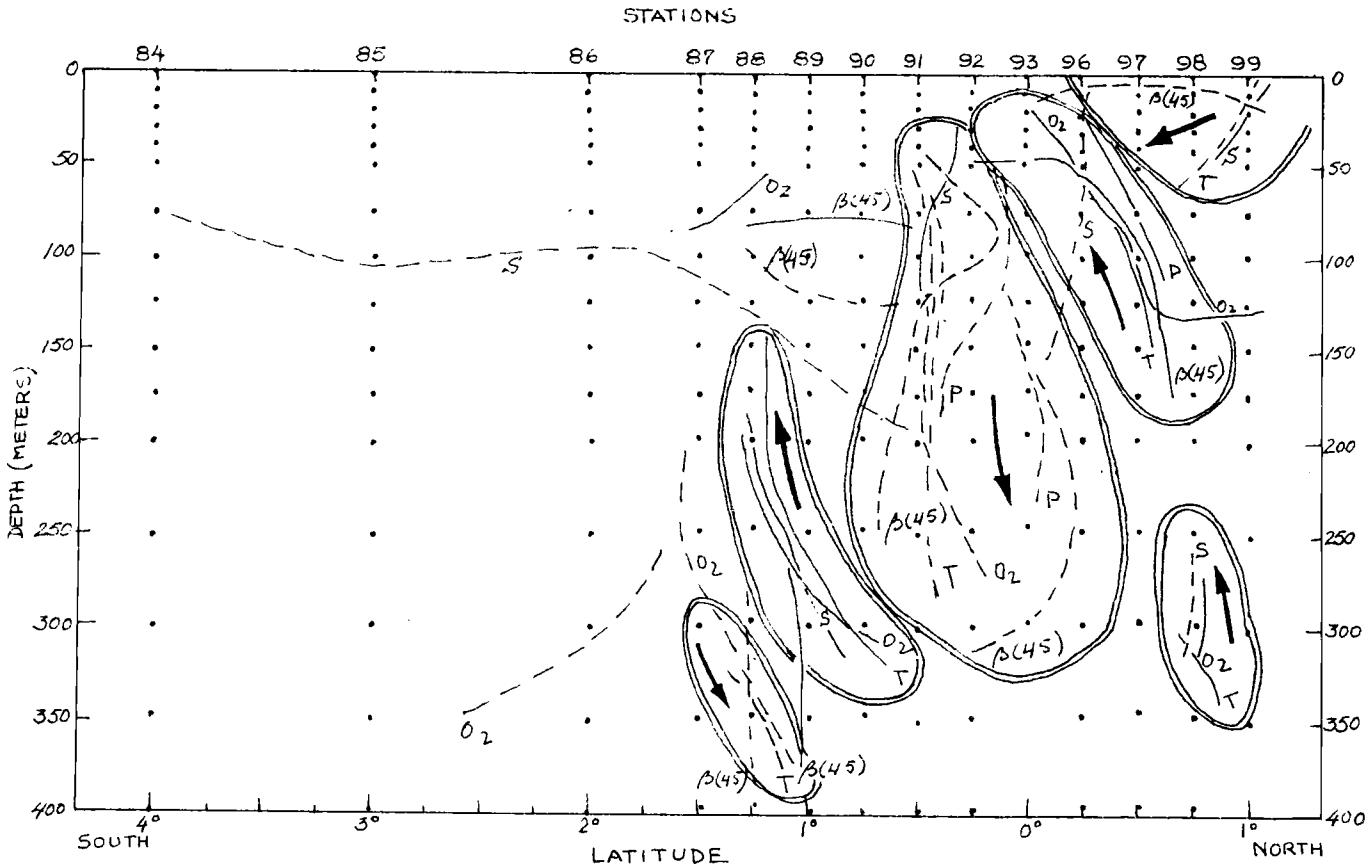

Figure 9. Local maxima (ridges) and minima (troughs) in the distributions of salinity (S), temperature (T), oxygen content (O_2), light scattering ($\beta(45)$), and total particle content (P), at 91°40' West. Maxima are indicated by dashed lines; minima by solid lines. Double lines enclose regions where advection or mixing is suggested. Arrows indicate average direction of maxima or minima.

A less clearly suggested region of upward motion or mixing exists at approximately 1°00'S between 150 and 300 m depth.

It is evident that the broad regions where upward and downward diffusion or advection are taking place at 92°00'W have changed just 20 miles downstream to narrow bands of advection or diffusion existing side by side. The bands are suggestive of circulation cells. The change in meridional circulation in so short a distance must be attributed to the modifying influence of the Galapagos islands. The Cromwell current in this region must be very turbulent (Knauss, 1966), so that mixing increases closer to the islands as will be shown in the next section. It is to be expected that the meridional circulation at 91°40'W will usually be different from that at 92°00'W as the increased mixing at 91°40'W and the existence of a boundary nearby must influence the flow. Further observations in the Galapagos area will show whether the observed modifications of the flow at 91°40'W as compared to 92°00'W are permanent features or fluctuate under the influence of large scale turbulence.

Evidence for Increased Mixing Near the Galapagos Islands

As had been mentioned earlier, isogram spreading has been recognized as one of the characteristic features of the Cromwell current regime. The decreased vertical gradients are sometimes ascribed to vertical advection alone (Forrester, 1964). Care must be

exercised in the interpretation of isogram spreading, as mixing may also play an important part (Knauss, 1966). Istoshin (1966) argues that isotherm spreading is due to eddy diffusion alone. In all probability it is safe to assume that isogram spreading is at least partially due to mixing.

If mixing increases as one approaches the islands, the vertical gradients at 91°40'W should be smaller than those at 92°00'W in the region of the thermocline. We will now show that this is indeed the case. The maximum vertical distance between the 18°C and the 20°C isotherms at 92°00'W is 30 meters. At 91°40'W the maximum vertical distance between the 18°C and the 20°C isotherms is 85 meters. The maximum vertical distance between the 3.0 ml/l and 3.5 ml/l oxygen isolines is only 25 meters at 92°00'W and 130 meters at 91°40'W. Light scattering displays a similar behavior. The maximum vertical distance between the 60×10^{-4} (m-steradian)$^{-1}$ and the 80×10^{-4} (m-steradian)$^{-1}$ light scattering isograms is 35 meters at 92°00'W and 150 meters at 91°40'W. The maximum vertical gradients of temperature, oxygen content and light scattering in the thermocline were thus reduced by factors of .35, .19, and .23 in the 20 miles separating 92°00'W and 91°40'W. The Cromwell current water at 91°40'W is thus much more homogeneous than that at 92°00'W. This change must at least partially be attributed to mixing.

Figure 10 shows the superposition of the oxygen distributions at

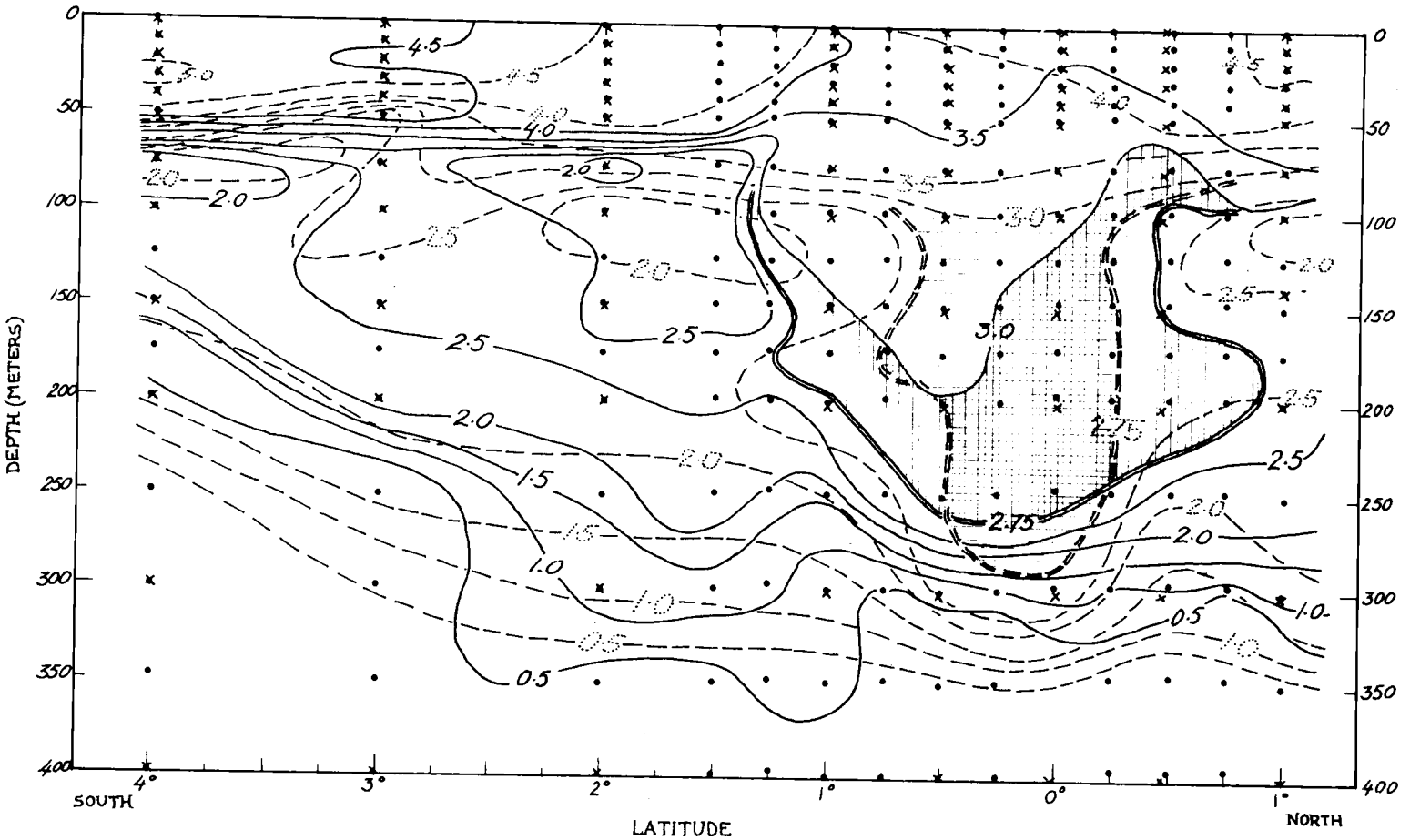

Figure 10. Superposition of oxygen content distributions at 92°00'W (dashed lines) and at 91°40'W (solid lines).

92°00'W and 91°40'W. It also shows the decreased gradient between 50 m and 100 m depth at 91°40'W as compared with 92°00'W as is evident from the greater separation of the isograms. A most interesting feature brought out by this figure is the widening and shallowing of the current at 91°40'W. This may be shown by comparing the regions enclosed by the 2.75 ml/l and the 3.0 ml/l isograms. At 92°00'W this region is approximately 70 miles wide and reaches a depth of 290 meters. At 91°40'W the region is 120 miles wide and reaches a depth of 260 meters.

Splitting of the Cromwell Current

There is evidence (Knauss, 1966; White, 1969) that the Cromwell current, although greatly weakened, continues to exist to the East of the Galapagos islands. Krauss (1966) shows that a deep eastward flowing current exists to the North of the Galapagos islands. He observed no such current to the South of the islands. White (1969) however, describes a southern branch of the Cromwell current which extends to the South American continent. If the current splits it must occur just West of the Galapagos islands, and should be apparent from the distribution of optical and hydrographic properties.

Montgomery (1962) indicates that the high velocity core of the Cromwell current coincides with the isotherm which is most nearly level. In our case the most level isotherm is the 20°C isotherm at

approximately 80 m depth. Due to the spreading of isograms in the Cromwell current the core should be identifiable by horizontal maxima of temperature, oxygen content and light scattering at 100 m depth. The horizontal distribution of these properties at 100 m depth will then enable us to trace the high velocity core of the Cromwell current as it approaches the islands. Figures 11, 12, and 13 show the distributions of temperature, oxygen content, and $\beta(45)$ at 100 m depth immediately West of the Galapagos islands.

The horizontal plots at 100 m show the existence of tongues of water with high temperature, oxygen content and light scattering to the Northwest and Southwest of Isla Isabela. These tongues are suggestive of a splitting of the current into a northern and a less clearly indicated southern branch.

The horizontal maxima at 92°00'W in temperature, oxygen content and $\beta(45)$ all occur to the South of the equator. This southward displacement of the high velocity core of the current may be ascribed to a southward oscillation of the Cromwell current. Such oscillations have been observed in the Atlantic equatorial undercurrent (Rinkel, 1969). Rinkel describes a North-South oscillation of at least 45 miles with a period of 11 days, and another observation of a 75 mile oscillation to the South over a 12 1/2 day period. A southward displacement of approximately 30 miles such as we observed is thus not unreasonable in the light of Rinkel's observations.

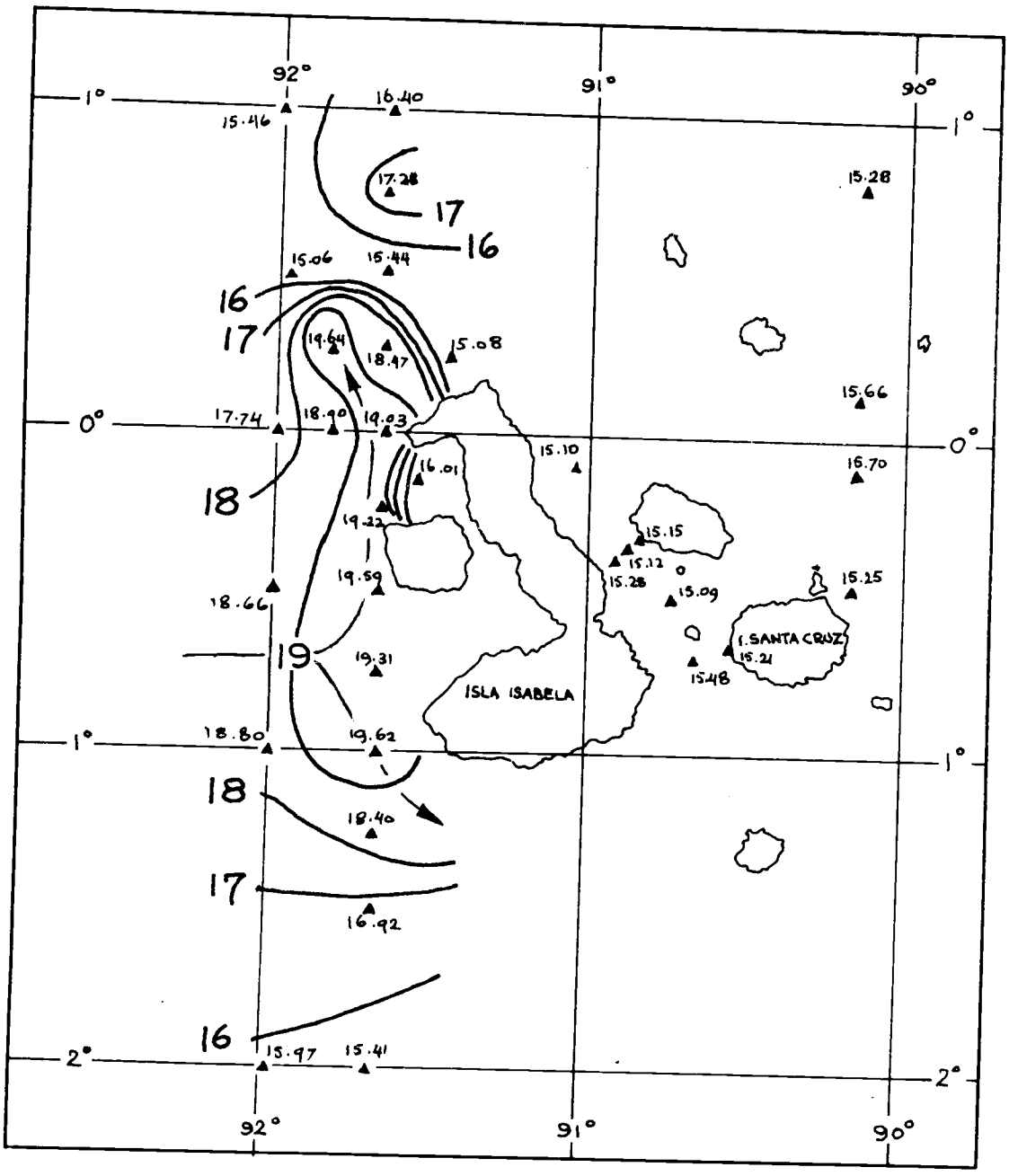

Figure 11. Temperature (°C) at 100 m depth.

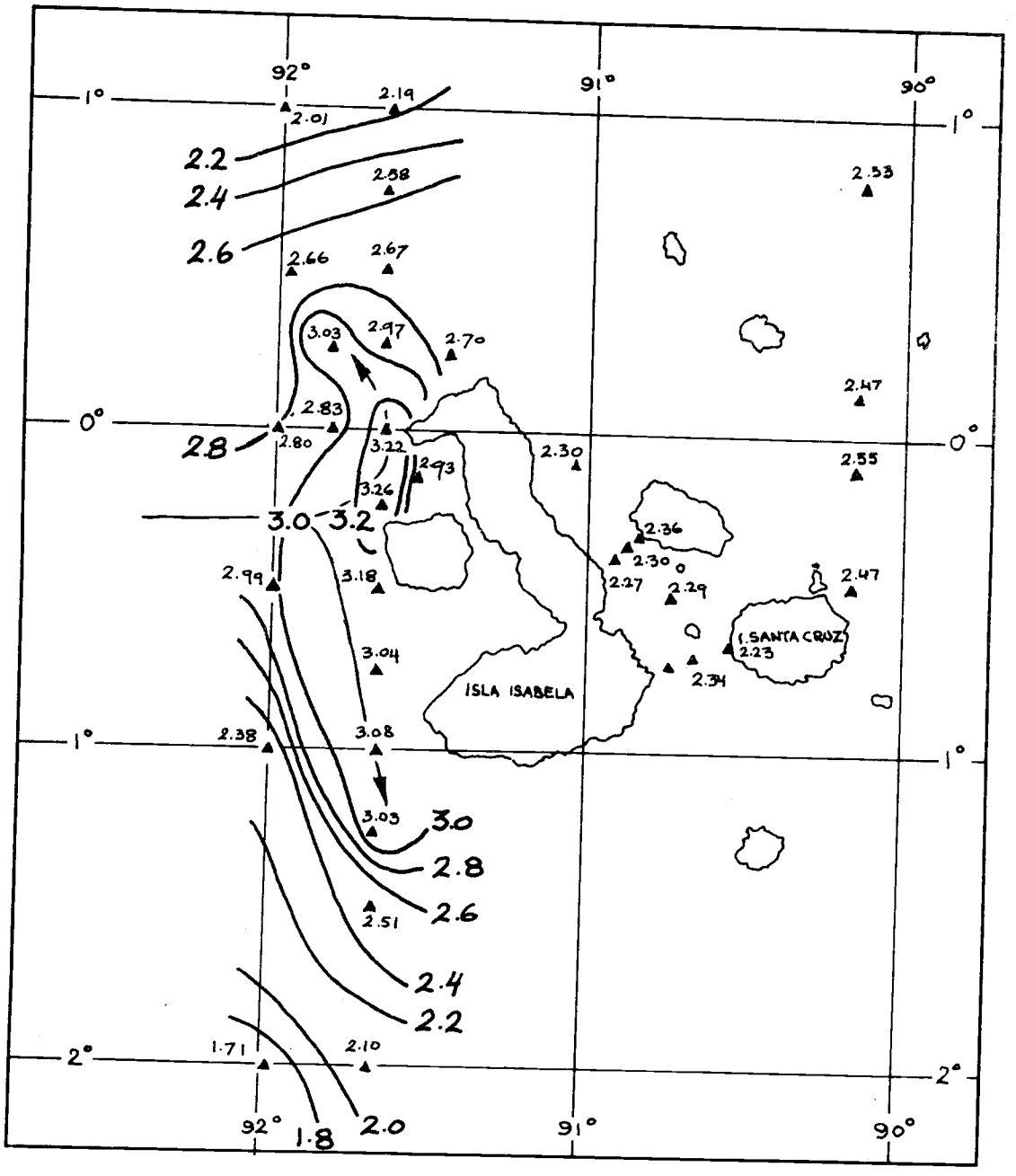

Figure 12. Oxygen content (ml/l) at 100 m depth.

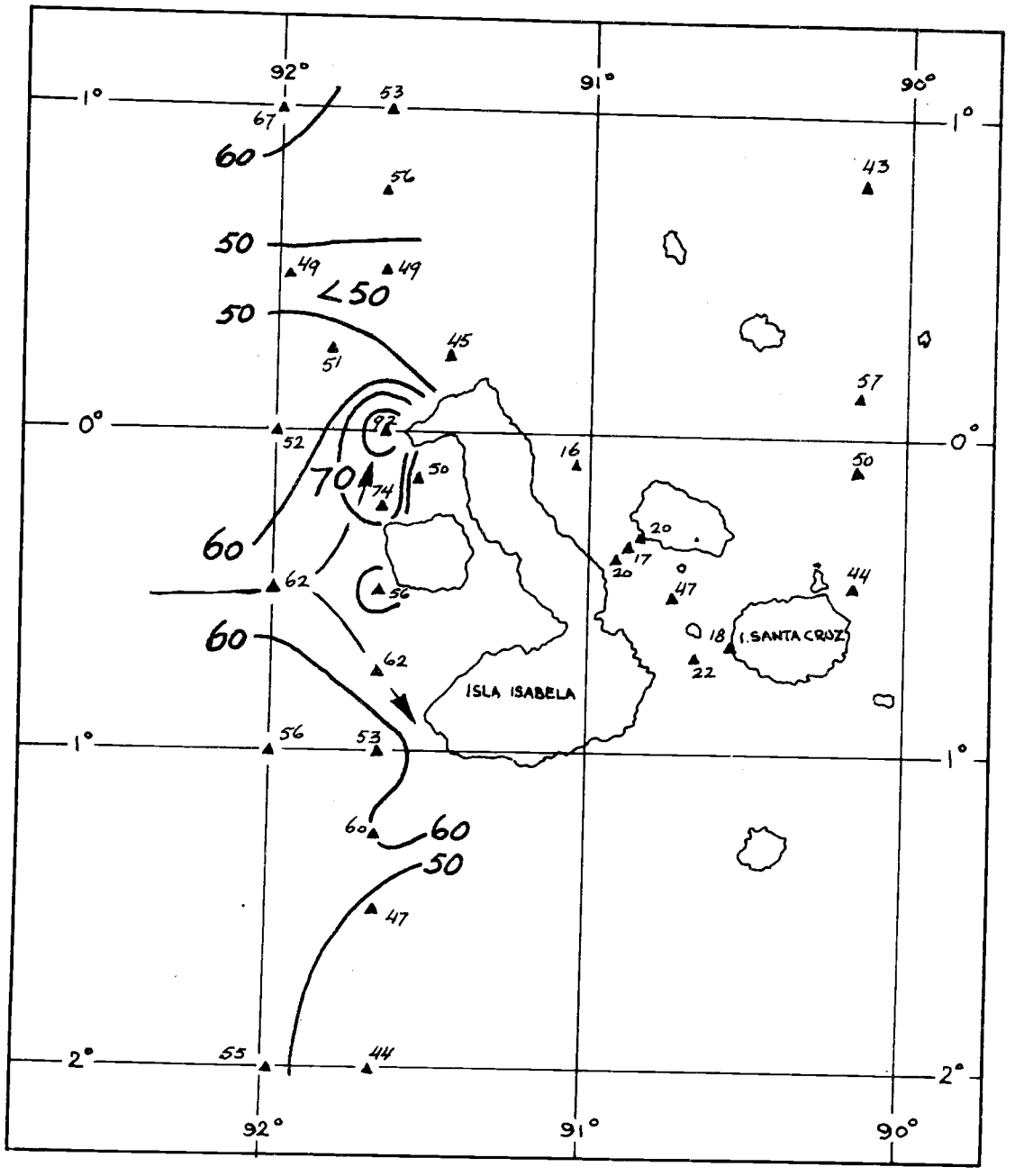

Figure 13. Light scattering at 45° $(m\text{-steradian})^{-1} \times 10^{-4}$ at 100 m depth.

An interesting observation is the existence of horizontally isolated maxima in temperature, oxygen content and light scattering just West of the Galapagos islands at 100 m depth. These maxima may be ascribed to isogram spreading due to increased turbulence near the islands, which was described earlier.

Evidence of Long Period Variations in the Cromwell Current

It is interesting to compare our drogue measurements with the current meter measurements of Knauss (1960, 1966). Knauss took current meter observations at 92°16'W in 1961. The maximum eastward velocity that he observed was 15 cm/sec at a depth of approximately 125 meters. In 1958 Knauss observed an eastward velocity of 50 cm/sec at 92°00'W. We released a drogue at 100 m depth 10 miles to the West of Isla Isabela at 0°00' and 91°40'W, and observed a velocity to the Northeast of approximately 50 cm/sec. The eastward velocity in the core of the current thus fluctuates greatly near the Galapagos islands.

We also observed higher salinities in the core near the Galapagos islands than Knauss (1966). Knauss observed salinities of 35.2‰ as far East as 110°W. Our salinity distribution at 91°40'W shows several pockets of 35.2‰ water (Figure 14). The core was thus more saline than during Knauss' observations. This observation correlates well with the current observations. Since the saline water originates

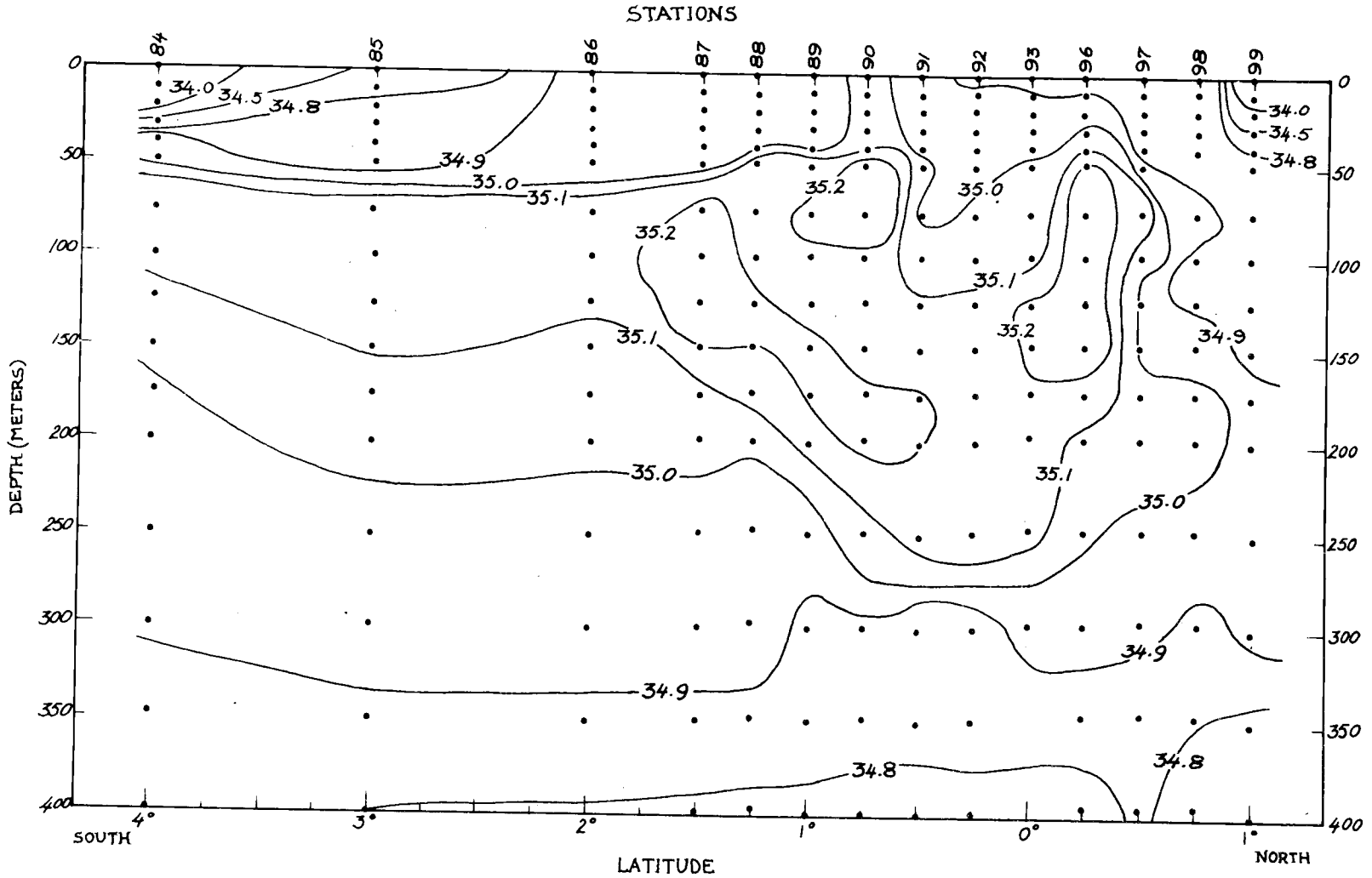

Figure 14. Salinity (‰) at 91°40'W longitude.

to the South and is then carried eastward by the Cromwell current, a more saline core is to be expected when the current speed is higher.

The pockets of 35.2‰ or higher salinities observed at 91°40'W are a major indication of temporal variations in the hydrographic properties of the Cromwell current. The maximum salinity observed at 92°00'W was 35.18‰ and at 91°40'W the maximum observed salinity was 35.44‰. The salinity difference was thus greater than .25‰ in a distance of about 20 miles. This observation seems to indicate that pockets of high salinity water are carried eastward by the Cromwell current. Since the current speed was about 1 knot, it is thus not unreasonable to expect variations of .25‰ salinity in one day at one place.

CONCLUSIONS

In the theoretical section we discussed the behavior of particles and particle size distributions in response to decay mechanisms and to mixing and advection. It was found that the particle concentration and hence light scattering can be related to advection and mixing in a way that is similar to the conservative properties of sea water. The optical properties can thus be used in the core method along with the usual hydrographic variables.

Decaying particles beneath the thermocline cause vertical gradients in light scattering. Deepening and shallowing of the light scattering isograms may thus be related to downward and upward motion of the water, respectively.

The core method, incorporating light scattering and particle counts, was then applied to the Cromwell current region between 92°00'W and the Galapagos islands.

The optical properties of the Cromwell current were identified. Beneath approximately 50 m depth deepening of the light scattering isograms occurred. Above this depth shallowing of the light scattering isograms was observed. A meridional surface minimum in light scattering existed above the region of the current. The particle concentration displayed basically the same properties as the light scattering.

In the region between 92°00'W and the Galapagos islands evidence was for a greatly modified meridional circulation as the Cromwell current approaches the islands. Increased mixing at 91°40'W as compared to 92°00'W is indicated by decreased vertical gradients of temperature, oxygen content and light scattering in the thermocline region. The core of the current may be traced by studying the horizontal distributions of temperature, oxygen and light scattering just beneath the level of maximum eastward velocity, as these properties display horizontal maxima at that level. Using this method it was found that the core of the current had widened considerably between 92°00'W and 91°40'W, indicating the splitting of the current in that area.

Pockets of high salinity water were observed in the current showing a possible variation of 0.25‰ salinity variation in one day in the same location.

BIBLIOGRAPHY

Beardsley, G.F., Jr. and J. R.V. Zaneveld. 1969. Theoretical dependence of the near-asymptotic apparent optical properties on the inherent optical properties of sea water. Journal of the Optical Society of America 59(4):373-377.

Bennett, E.B. 1963. An oceanographic atlas of the eastern tropical Pacific ocean, based on data from the EASTOPAC Expedition, Oct.-Dec. 1955. Inter-American Tropical Tuna Commission Bulletin 8(2):165 pp.

Buchanan, J.Y. 1886. On similarities in the physycal geography of the great oceans. Proceedings of the Royal Geographic Society 8:753-770.

Buchanan, J.Y 1888. The exploration of the Gulf of Guinea. Scottish Geographic Magazine 4:177-200; 232-251.

Burt, W.V. 1956 A light-scattering diagram. Journal of Marine Research 15:76-80.

Carder, L.C. 1970. Particles in the eastern Pacific Ocean: their distribution and effect upon optical parameters. Ph.D. thesis. Corvallis, Oregon State University. 140 numb. leaves.

Charney, J.G. 1960. Non-linear theory of a wind-driven homogeneous layer near the equator. Deep-Sea Research 6:303-310.

Cromwell, T., R.B. Montgomery and E.D. Stroup. 1954. Equatorial undercurrent in the Pacific Ocean revealed by new methods. Science 119:648-649.

Forrester, W.D. 1964. Thermocline structure in the equatorial Pacific. Journal of Marine Research 22:142-151.

Hidaka, K. 1966. Non-linear computation of the equatorial upwelling. Oceanographic Society of Japan, Tokyo, Journal 22:145-153.

Hisard, P. et al. 1969. Comparison of the equatorial waters North of New Guinea and at 170°E. Journal of Marine Research 27:191-205.

Ichiye, T. 1964. An essay on the equatorial current system. In: ed K. Yoshida Studies on Oceanography. Seattle, University of Washington. pp. 33-46.

Ichiye, T. 1966a. Turbulent diffusion of suspended particles near the ocean bottom. Deep-Sea Research 13:679-685.

Ichiye, T. 1966b. Vertical currents in the equatorial Pacific ocean. Oceanographic Society of Japan, Tokyo, Journal 22:274-284.

Istoshin, Yu. V. 1966. Features of water temperature distribution in the pre-equatorial zone of the Pacific Ocean. Translated from the Russian. Oceanology 6:36-41.

Jerlov, N.G. 1951. Optical studies of ocean water. Reports of the Swedish Deep-Sea Expedition 3:1-59.

Jerlov, N.G. 1953. Particle distribution in the ocean. Reports of the Swedish Deep-Sea Expedition 3:73-97.

Jerlov, N.G. 1959. Maxima in the vertical distribution of particles in the sea. Deep-Sea Research 5:173-184.

Jerlov, N.G. 1968. Optical oceanography. Elsevier, Amsterdam. 194 pp.

Joseph, J. 1955. Extinction measurements to indicate distribution and transport of ocean masses. Proceedings of the U.N.E.S.C.O. Symposium on Physical Oceanography, Tokyo, pp. 59-75.

Knauss, J.A. 1960. Measurements of the Cromwell Current. Deep-Sea Research 6:265-286.

Knauss, J.A. 1966. Further measurements and observations on the Cromwell Current. Journal of Marine Research 24:205-239.

Long, R.R. 1961. A turbulent equatorial jet. Journal of Fluid Mechanics 11:465-469.

Metcalf, W.G., A.D. Voorhis and M.C Stalcup. 1962. The Atlantic equatorial undercurrent. Journal of Geophysical Research 67:2499-2503.

Mie, G. 1908. Beiträge zür optik trüber medien, speziell kolloidalen metallösungen. Annalen der Physik 25:377.

Montgomery, R.B. 1962. Equatorial undercurrent observations in review. Journal of the Oceanographic Society of Japan, 20th anniversary Volume:487-498.

Neumann, G. 1966. Equatorial undercurrent in the Atlantic Ocean. In: Symposium on the Oceanography and Fishery Resources of the Tropical Atlantic, Abidjan Ivory Coast Oct. 20-28, 1966. Proceedings: Review papers and contributions. Paris, U.N.E.S.C.O. pp. 33-44.

Pak, H. 1969. The Columbia River as a source of marine light scattering particles. Ph.D. thesis. Corvallis, Oregon State University, 110 numb. leaves.

Pak, H., G.F. Beardsley, Jr. and P.K. Park. 1970. The Columbia River as a source of marine light scattering particles. Journal of Geophysical Research 75:2837-2845.

Pak, H., J.R.V. Zaneveld and G.F. Beardsley, Jr. 1971. Mie scattering by suspended clay particles. Journal of Geophysical Research. (In press).

Pond, S., R.M. Pytkowicz and J.E. Hawley. 1971. Particle dissolution during settling in the oceans. Deep Sea Research. (In press).

Prandtl L. and O.G. Tietjens. 1957. Applied hydro- and aerodynamics. Dover, New York, 311 pp.

Riley, G.A., H. Stommel and D.F. Bumpus. 1949. Quantitative ecology of the plankton of the western North Atlantic. Bulletin of the Bingham Oceanographic Collection 12:1-169.

Rinkel, M.O. 1969. Some features of relationships between the Atlantic equatorial undercurrent and its associated salinity core. In: Symposium on the Oceanography and Fisheries Resources of the Tropical Atlantic, Abidjan, Ivory Coast Oct. 29-28, 1966. Proceedings: Review Papers and Contributions. Paris, U.N.E.S.C.O., p. 193-212.

Robinson, A.R. 1960. The general thermal circulation in the equatorial regions. Deep-Sea Research 6:311-317.

Robinson, A.R. 1966. An investigation into the wind as the cause of equatorial undercurrent. Journal of Marine Research 24:179-204.

Swallow, J. C. 1964. Equatorial undercurrent in the western Indian Ocean. Nature 204(4957):436-437.

Taft, B. A. 1967. Equatorial currents. American Geophysical Union-Transactions 48:569-572.

Takano, K. 1967. K. Hidaka: Non-linear computation of the equatorial upwelling. Oceanographic Society of Japan, Tokyo, Journal 23:39-41.

Van De Hulst, H. C. 1957. Light scattering by small particles. Wiley, New York. 470 pp.

White, W. B. 1969. The equatorial undercurrent, the South equatorial countercurrent, and their extensions in the South Pacific Ocean East of the Galapagos Islands during February-March, 1967. College Station, Texas A & M University. 74 pp.

Wooster, W. S. and F. Jennings. 1955. Exploratory oceanographic observation in the eastern tropical Pacific. January to March, 1953. California Fish and Game 41:79-90.

Wooster, W. S. and T. Cromwell. 1958. An oceanographic description of the eastern tropical Pacific. Bulletin of the Scripps Institute of Oceanography 7, No. 3. p. 169-182.

Wyrtki, K. 1950. Über die Beziehungen zwischen Trübung und ozeanographischem aufbau. Kieler Meeresforschungen., Institut fur Meereskunde 7:87-107.

Wyrtki, K. 1962. The oxygen minima in relation to ocean circulation. Deep-Sea Research 9:11-23.

Wyrtki, K. and E. B. Bennett. 1963. Vertical eddy viscosity in the Pacific equatorial undercurrent. Deep-Sea Research 10:449-455.

Yoshida, K. 1967. Circulation in the eastern tropical oceans with special reference to upwelling and undercurrents. Japanese Journal of Geophysics Vol. 4, No. 2:1-75.

Zaneveld, J. R. V., M. Andrade and G. F. Beardsley, Jr. 1969. Measurements of optical properties at an oceanic front observed near the Galapagos Islands. Journal of Geophysical Research 74:5540-5541.

Zaneveld, J.R.V. and G.F. Beardsley, Jr. 1969. Modulation transfer function of sea water. Journal of the Optical Society of America 59(4):378-380.

Zaneveld, J.R.V., R. Hodgson and G.F. Beardsley, Jr. 1970. Image degradation over sea water paths - A review. AGARD Conference proceedings No. 77. Electromagnetics of the sea. AGARD-cp-77-70.

APPENDIX

APPENDIX

Distributions of Variables at 92°00'W, 91°40'W, 0 m, 100 m, or 200 m Depth, Not Referred to in the Text

The measured or calculated variables were salinity, temperature, oxygen content, density, light scattering at 45° from the forward and total particle count per cc for particles with a diameter greater than 2.2 microns. For all these variables plots were made of the meridional distributions at 92°00' West and at 91°40' West. Horizontal distributions are given at 0 m, 100 m, and at 200 meters depth. Some of the plots appeared in the text. Those that did not are included in this Appendix.

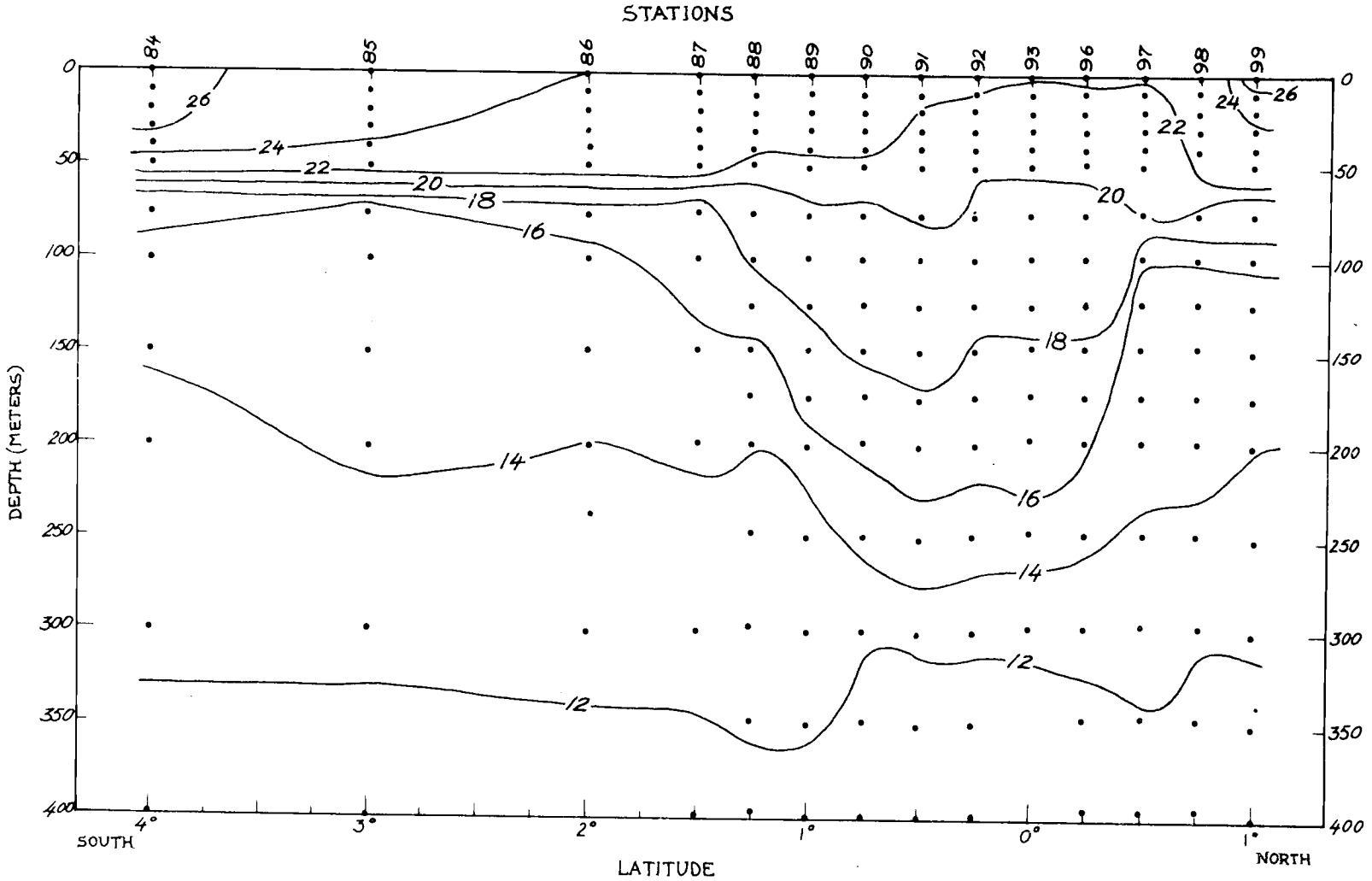

Figure 15. Temperature (°C) at 91°40'W longitude.

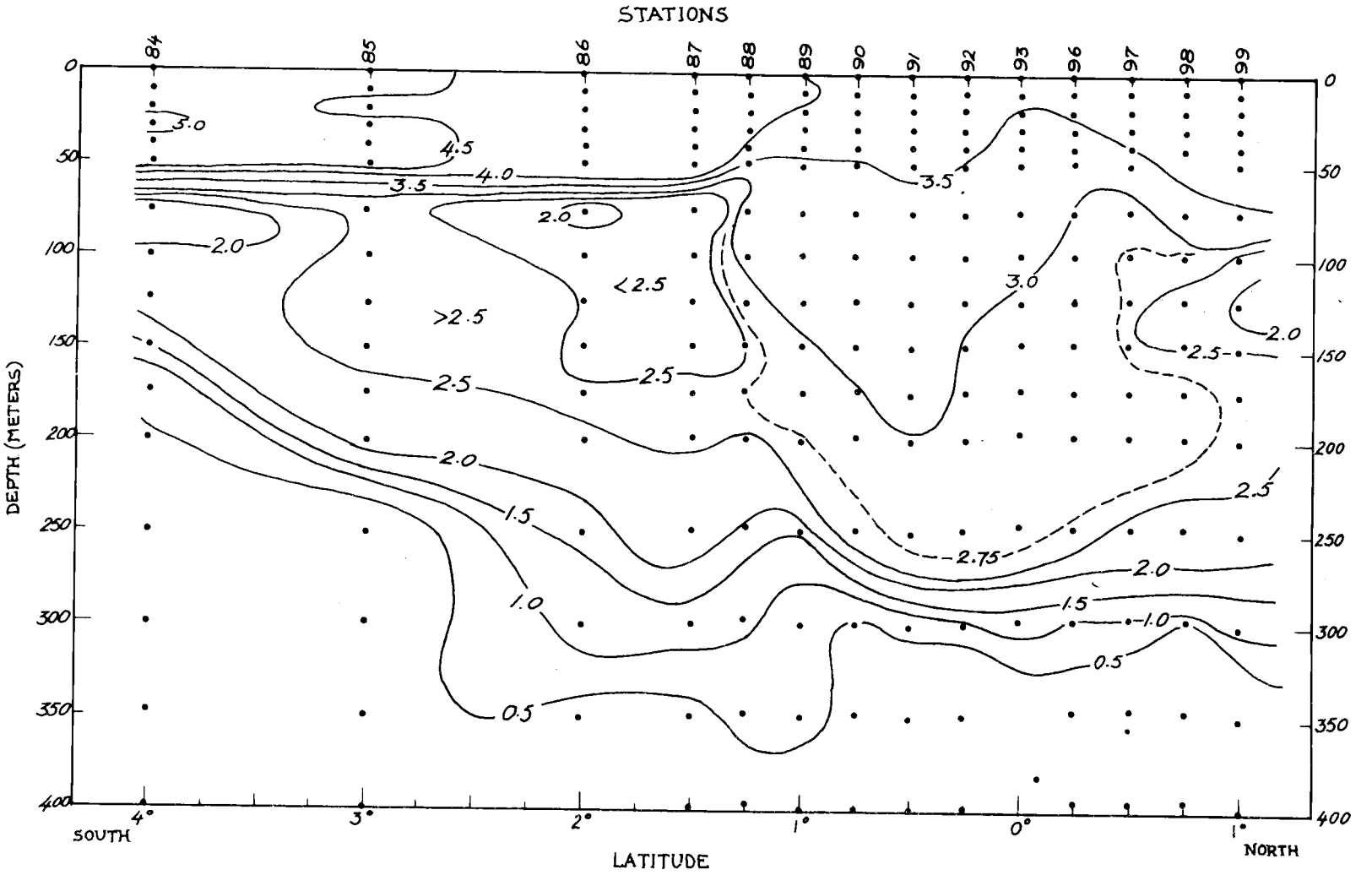

Figure 16. Oxygen content (ml/l) at 91°40'W longitude.

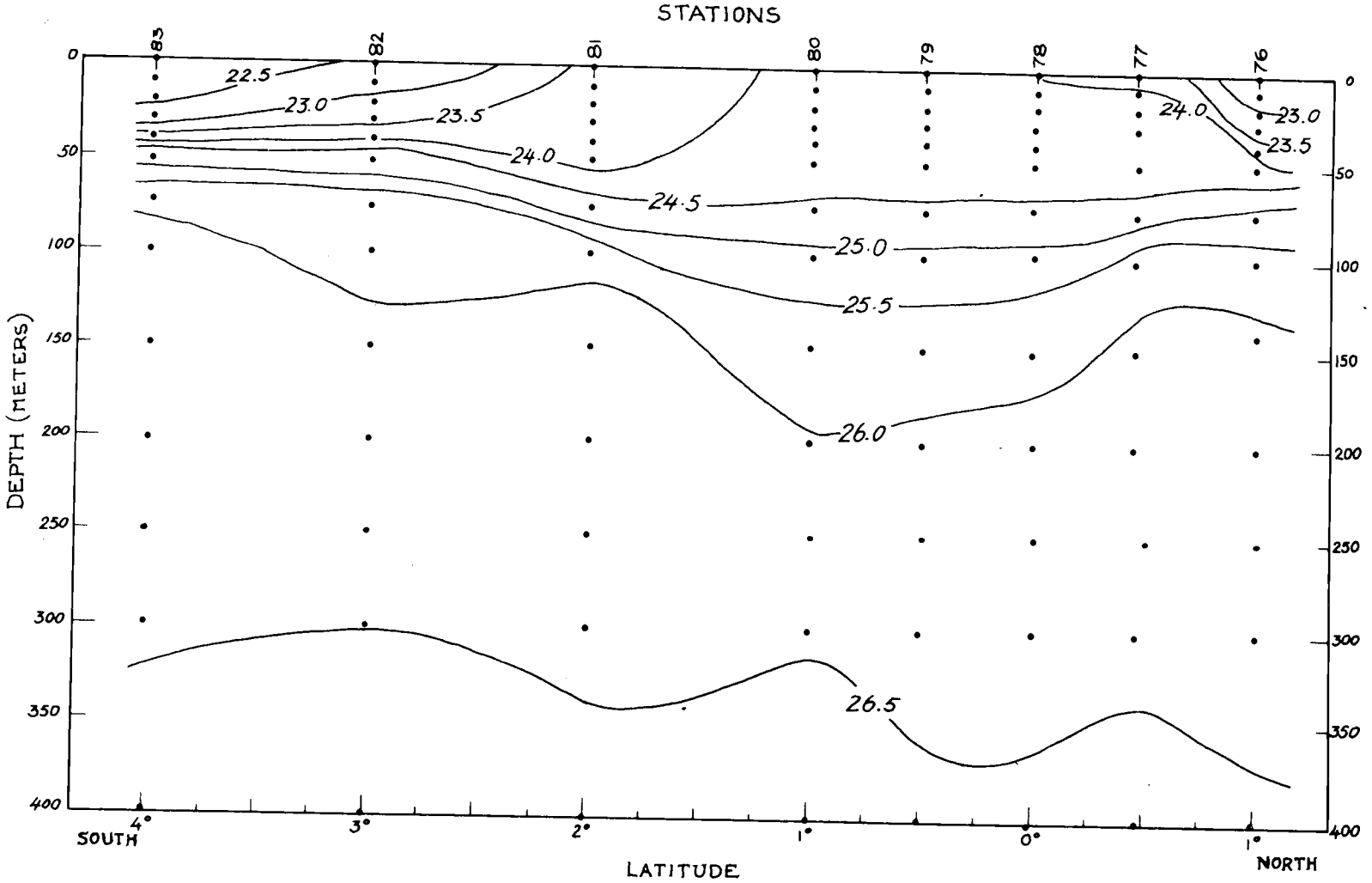

Figure 17. Density (units of σ_t) at 92°00'W longitude.

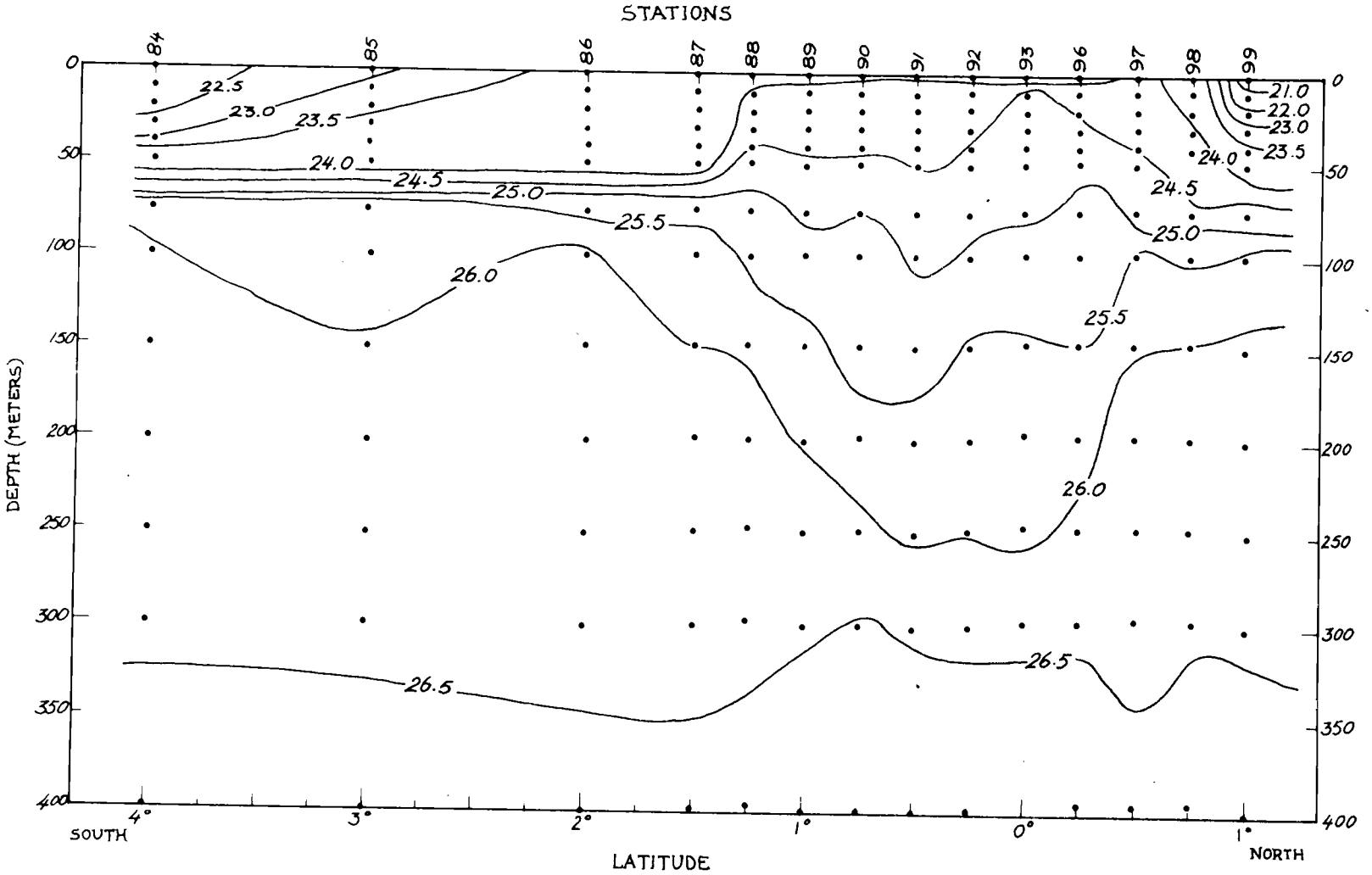

Figure 18. Density (units of σ_t) at 91°40'W longitude.

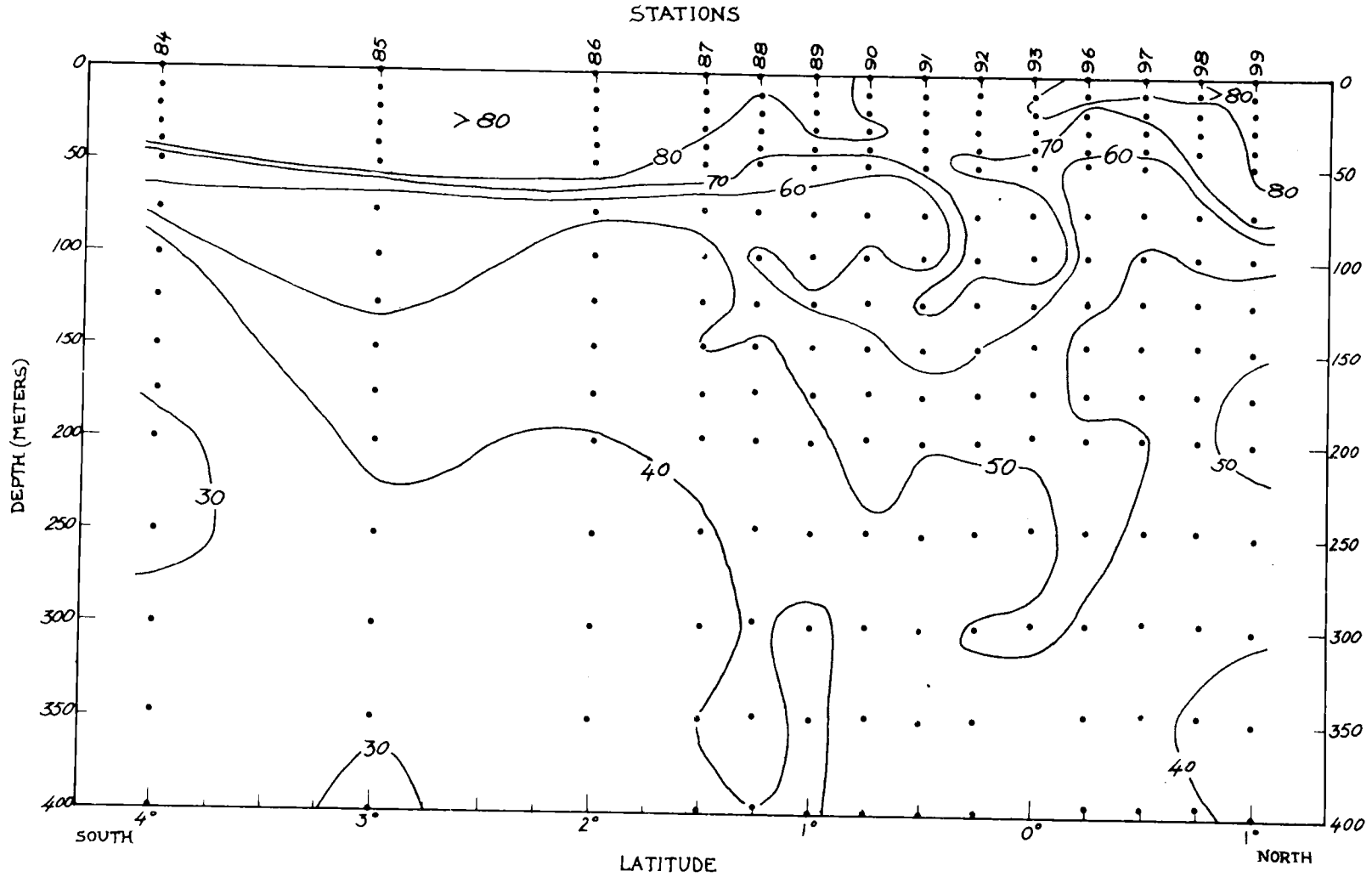

Figure 19. Light scattering at 45° $(\text{m-steradian})^{-1} \times 10^{-4}$ at 91°40'W longitude.

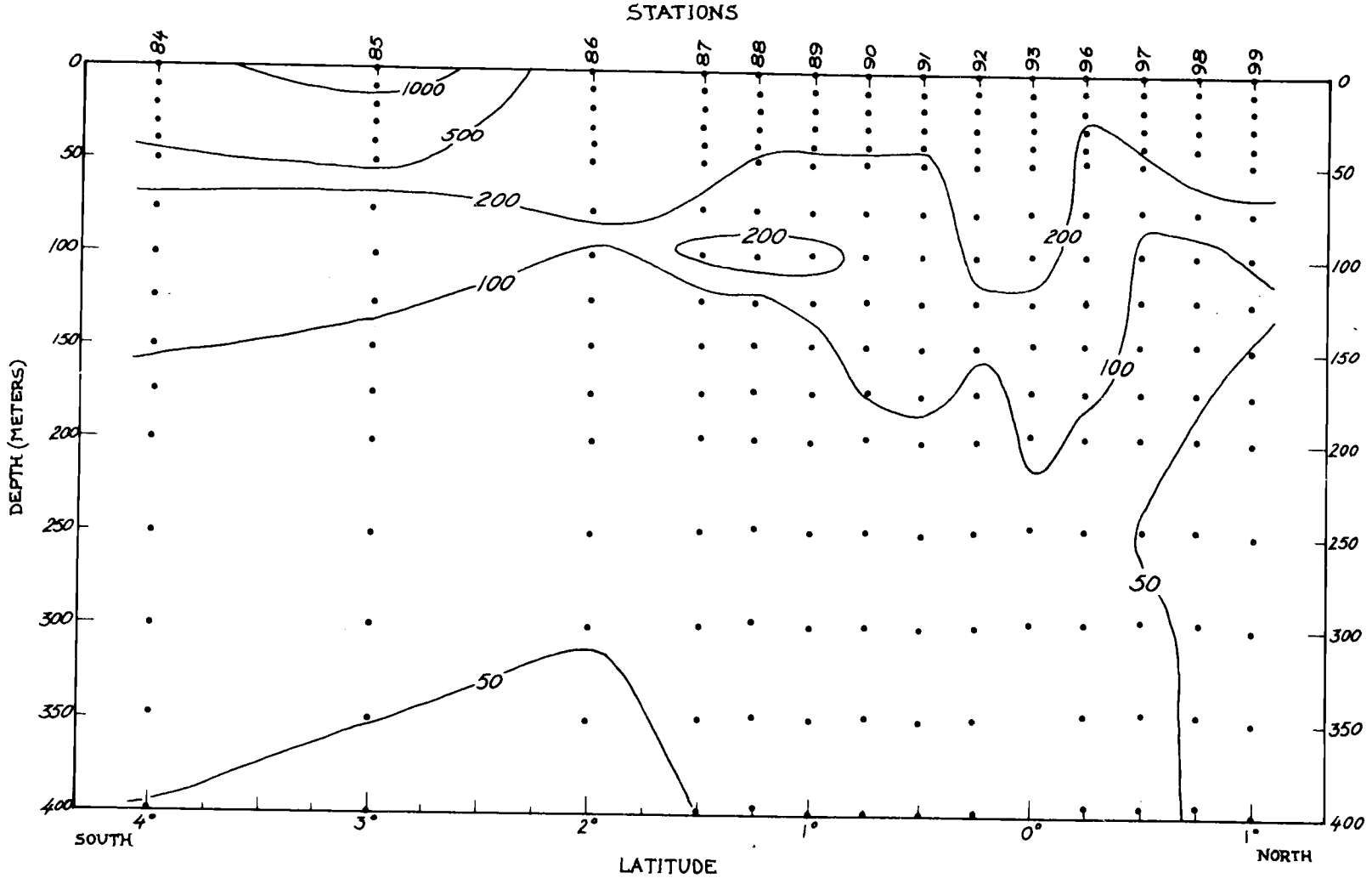

Figure 20. Total particle content per cc for particles with diameters greater than 2.2μ at 91°40'W.

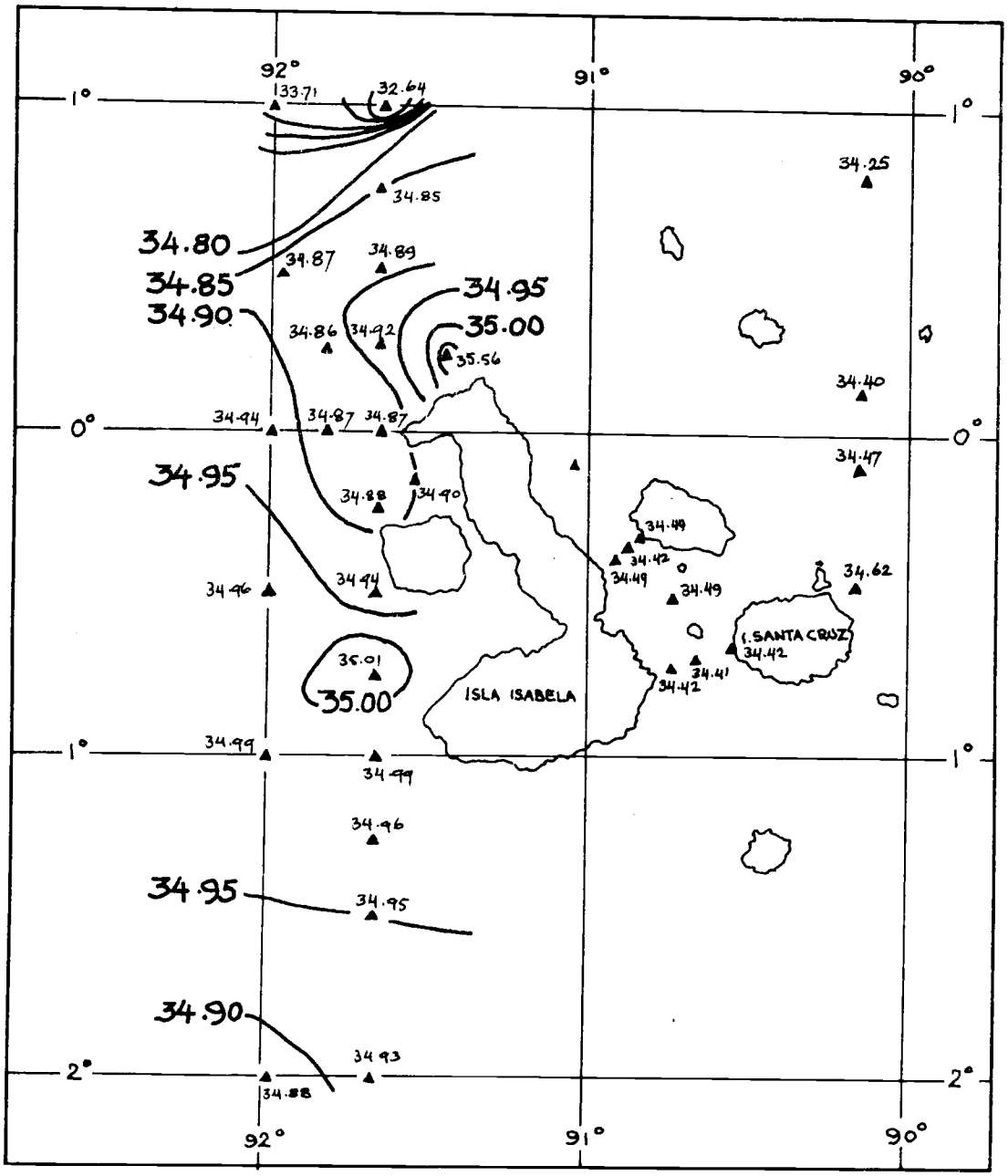

Figure 21. Salinity (‰) at 0 m depth.

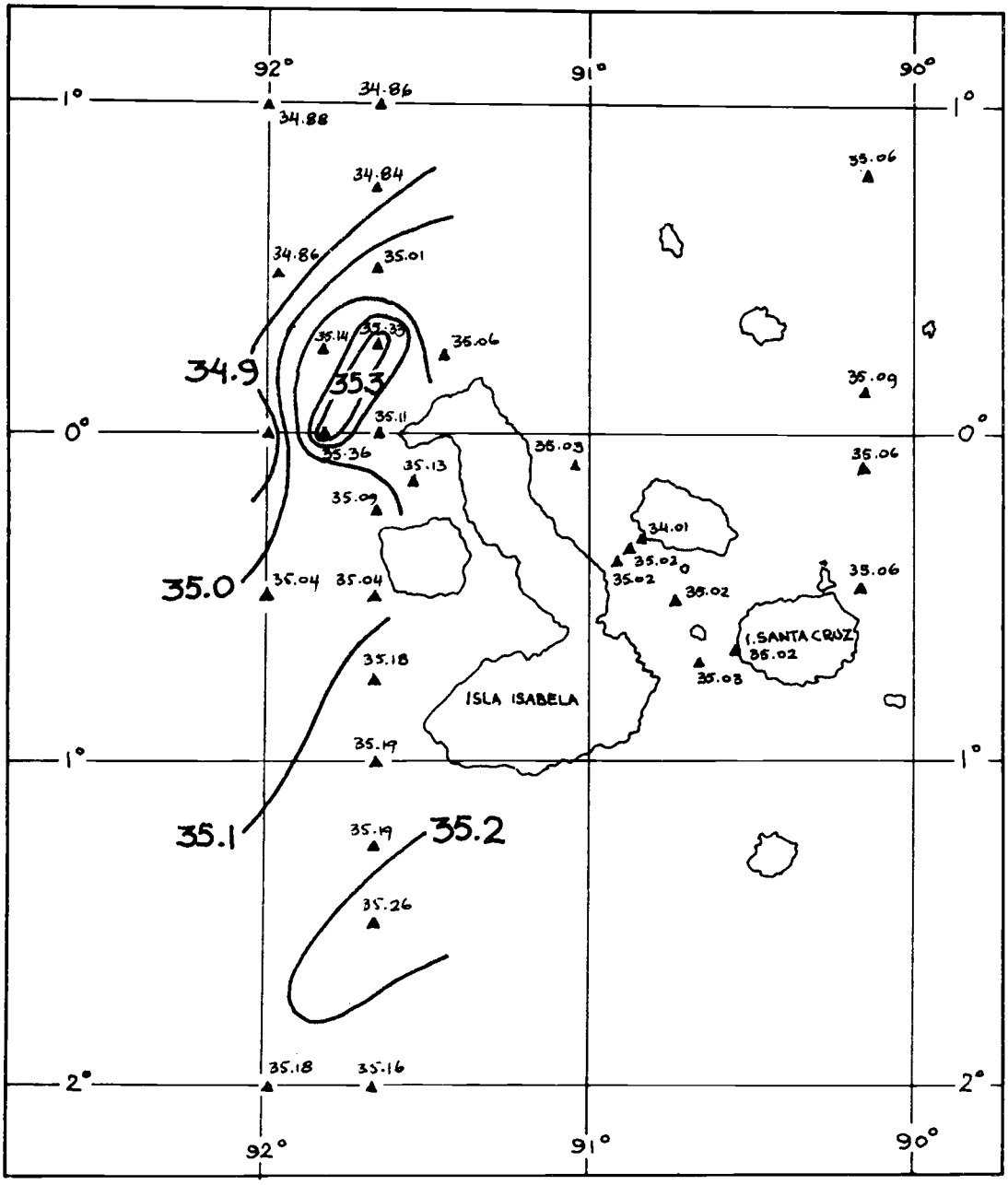

Figure 22. Salinity (‰) at 100 m depth.

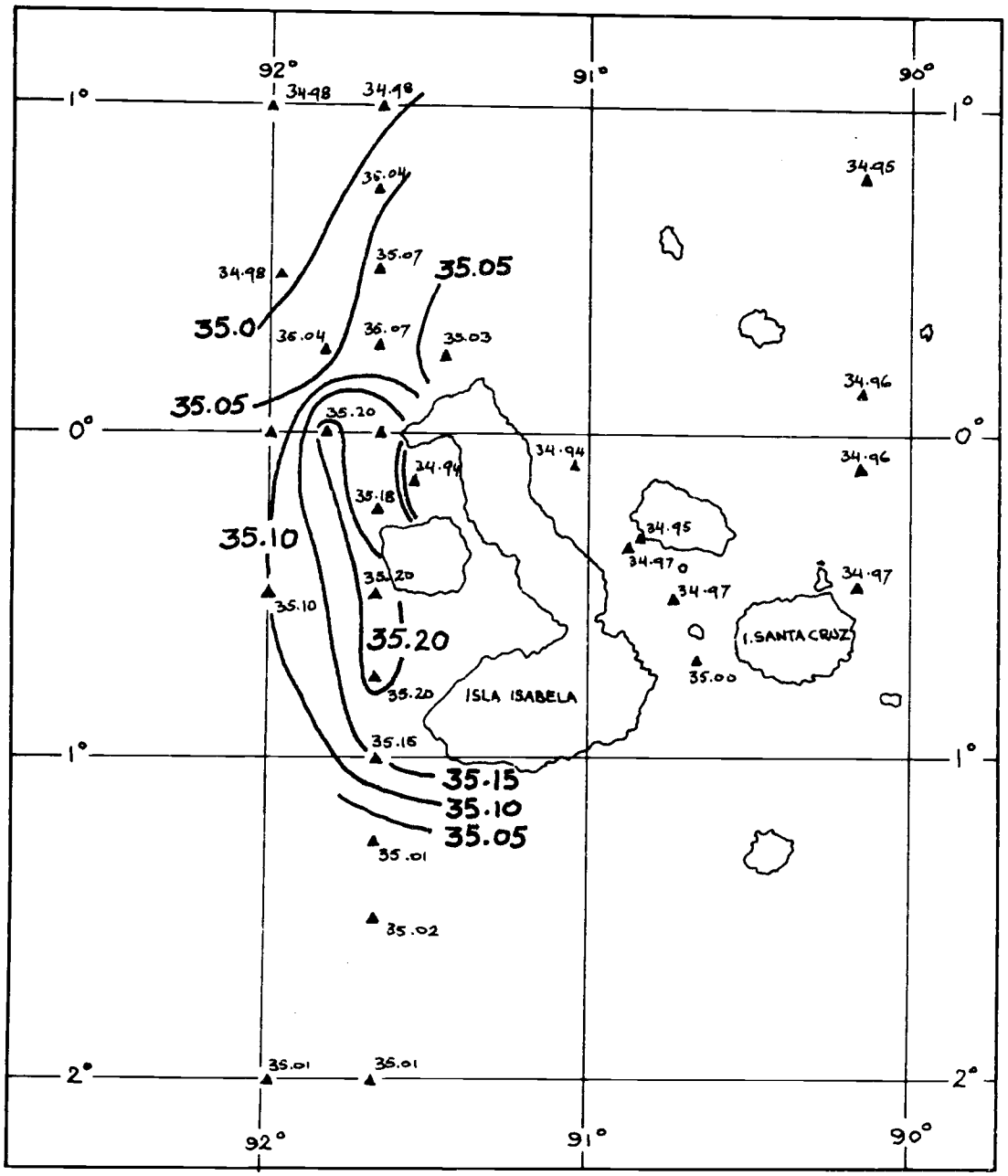

Figure 23. Salinity (‰) at 200 m depth.

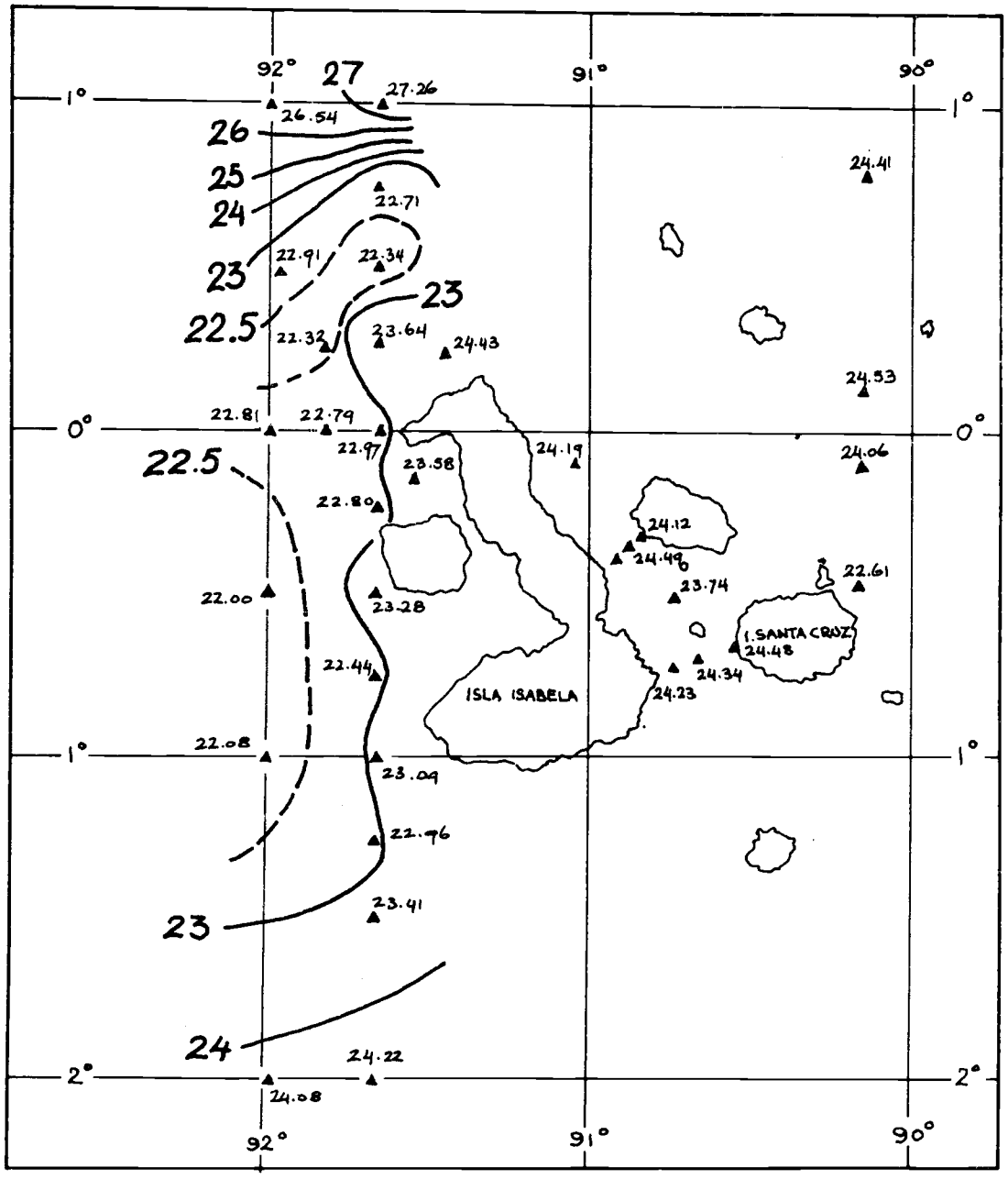

Figure 24. Temperature (°C) at 0 m depth.

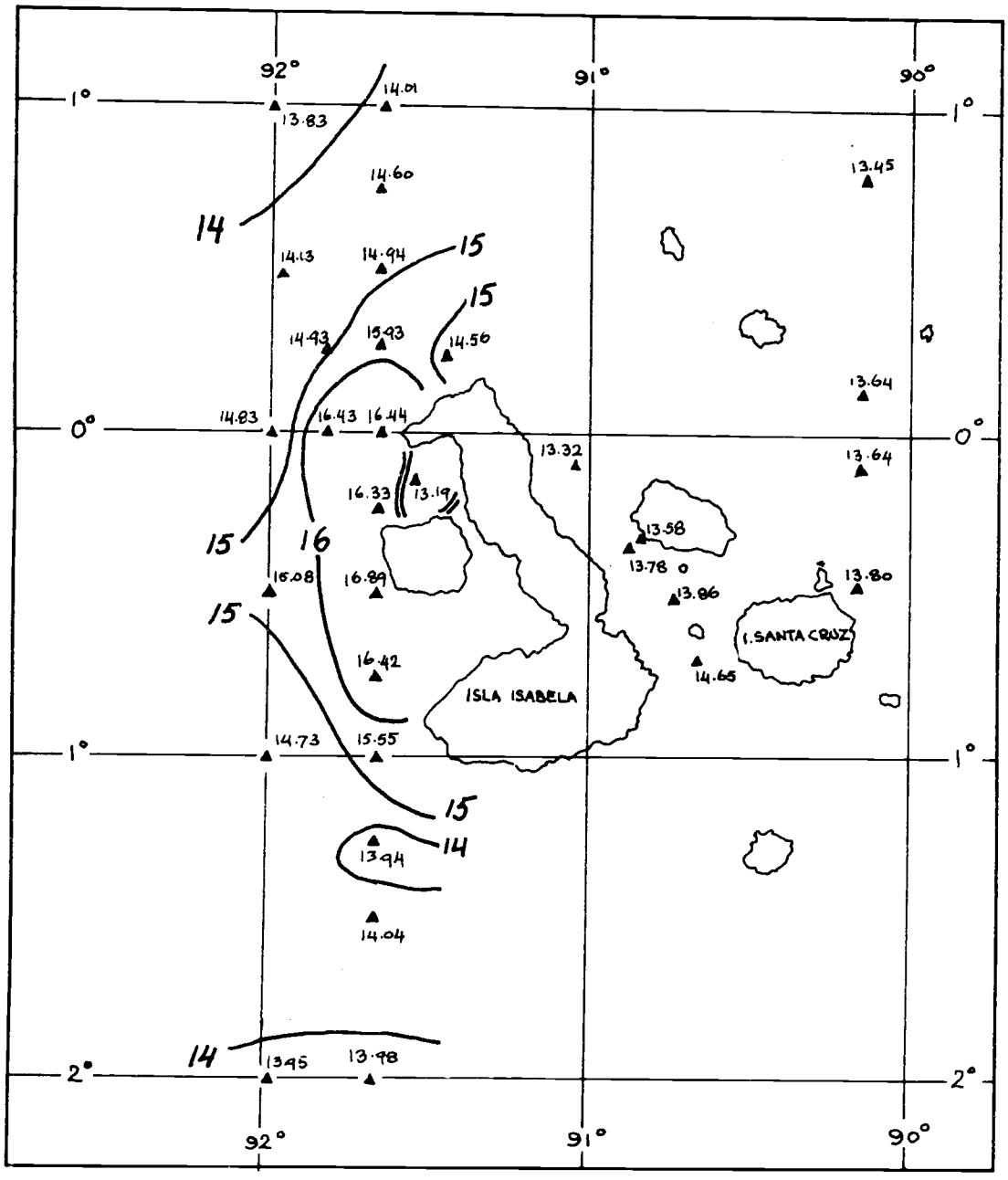

Figure 25. Temperature (°C) at 200 m depth.

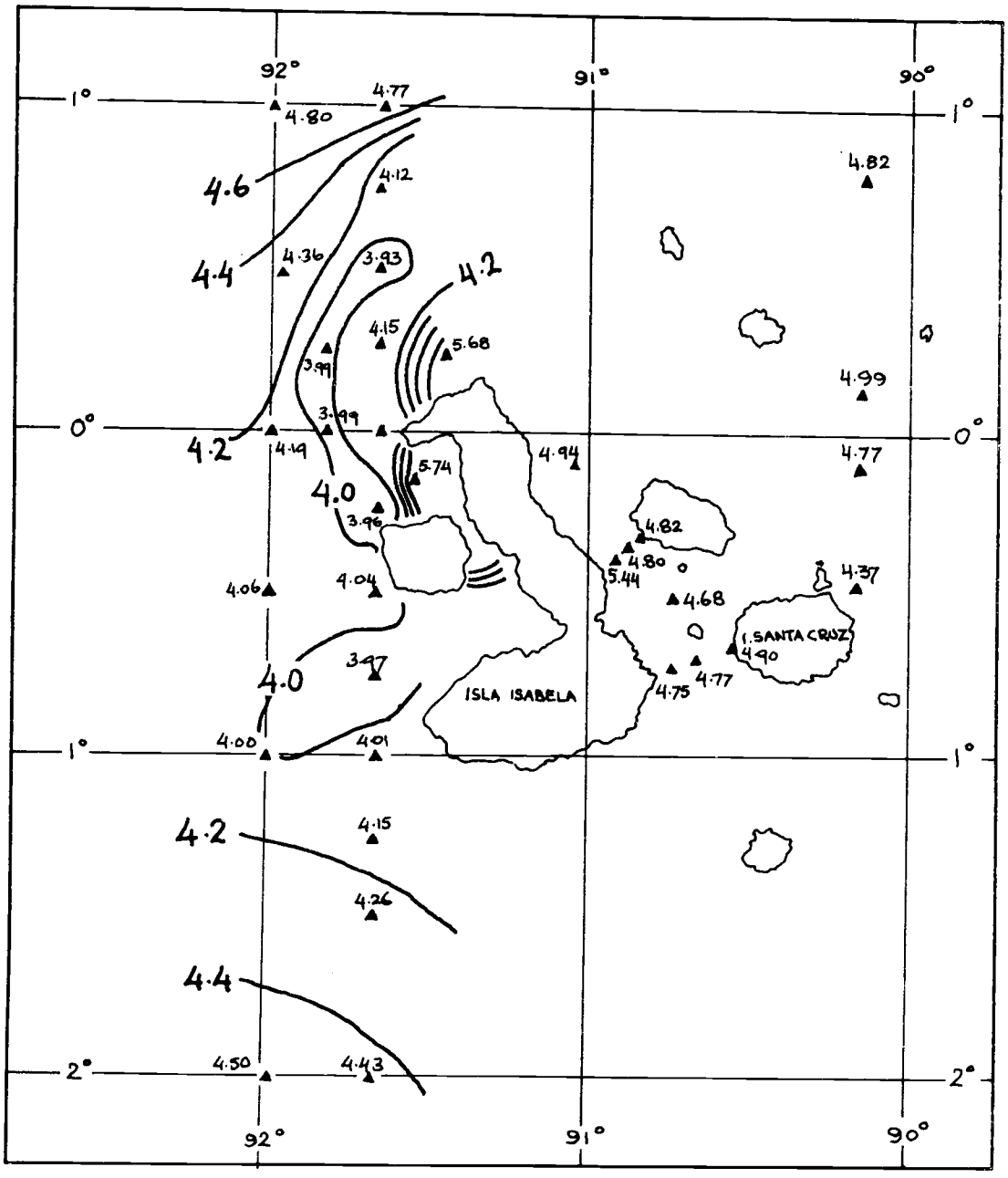

Figure 26. Oxygen (ml/l) at 0 m depth.

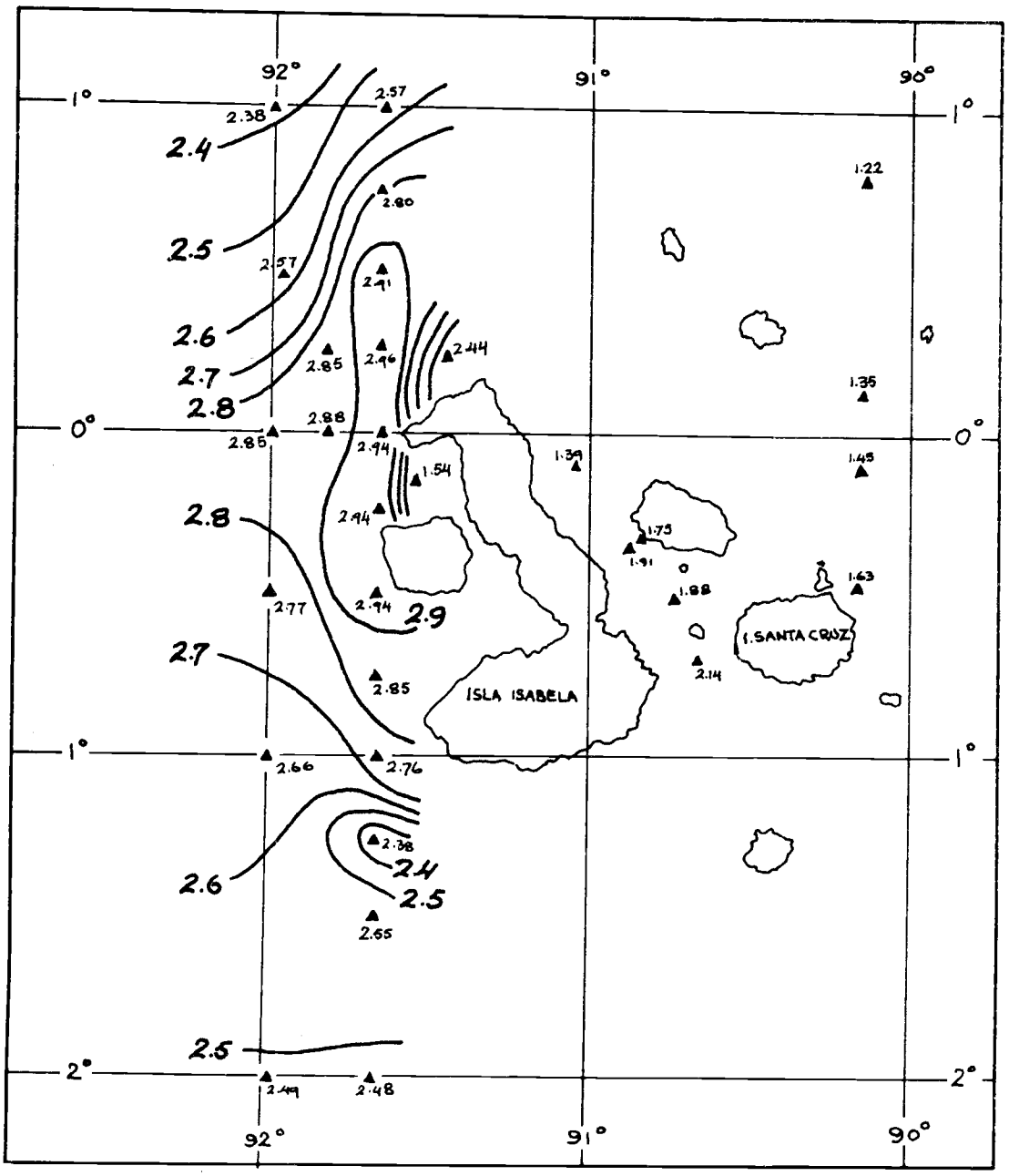

Figure 27. Oxygen (ml/l) at 200 m depth.

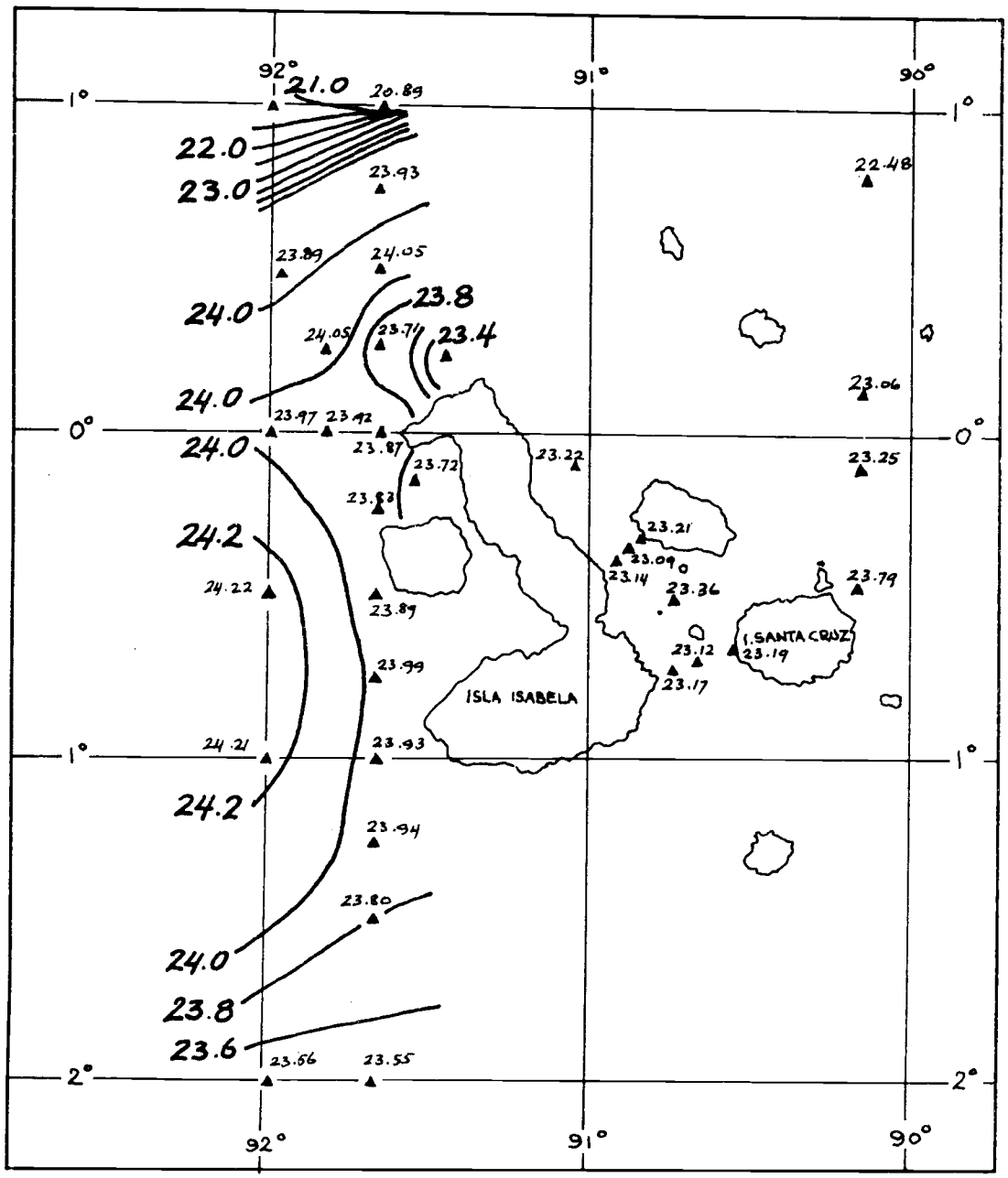

Figure 28. Specific gravity (σ_t) at 0 m depth.

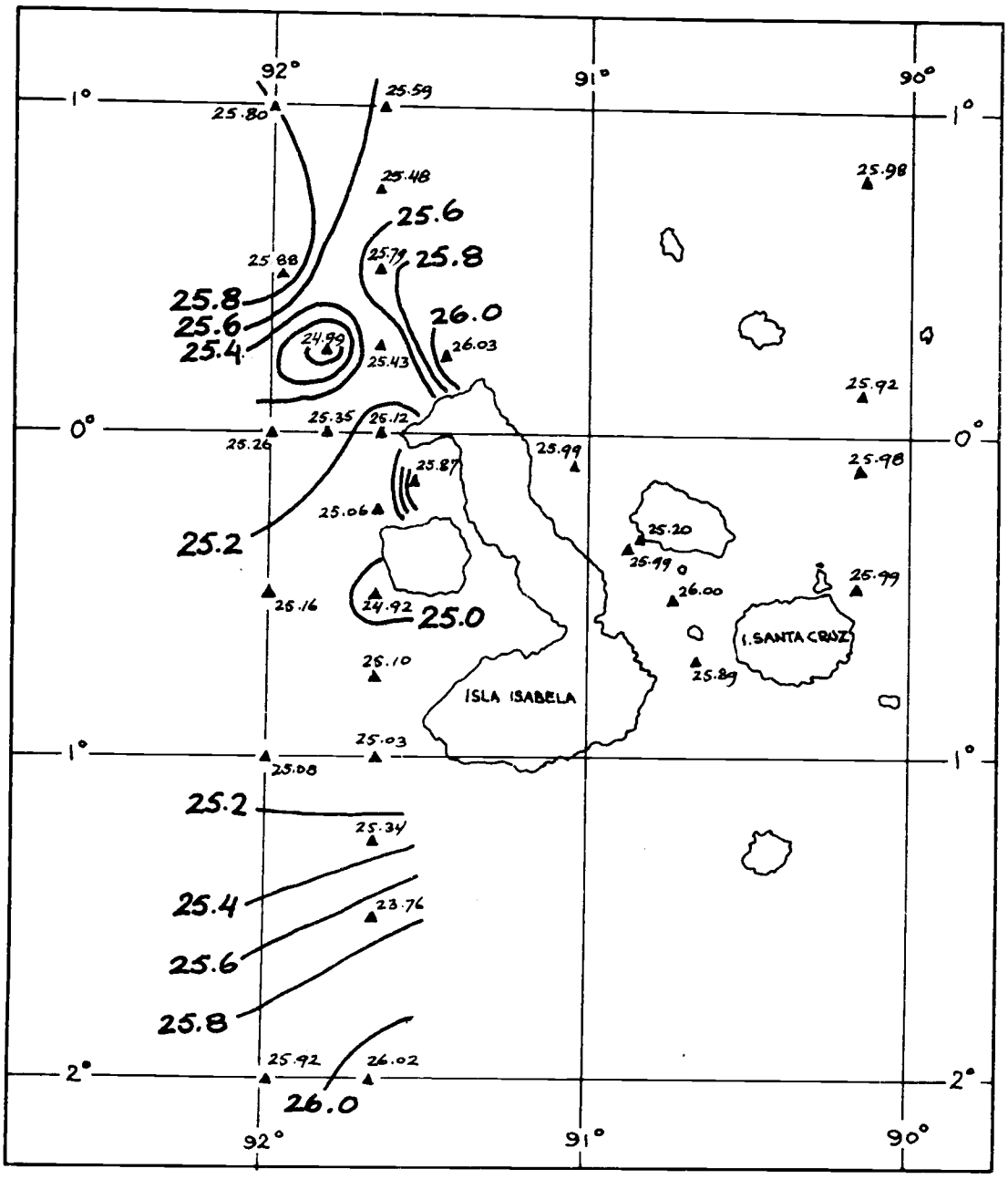

Figure 29. Specific gravity (σ_t) at 100 m depth.

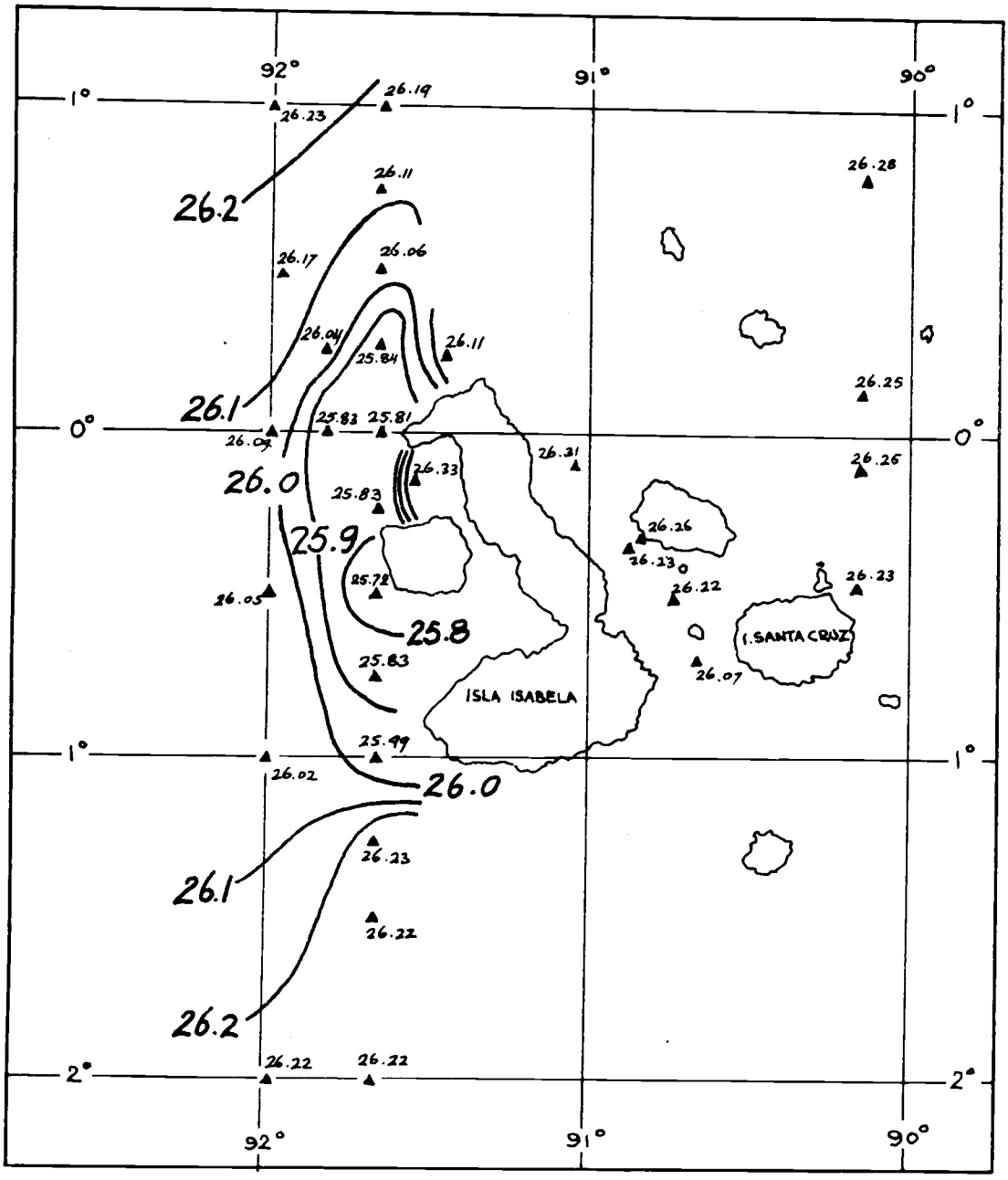

Figure 30. Specific gravity (σ_t) at 200 m depth.

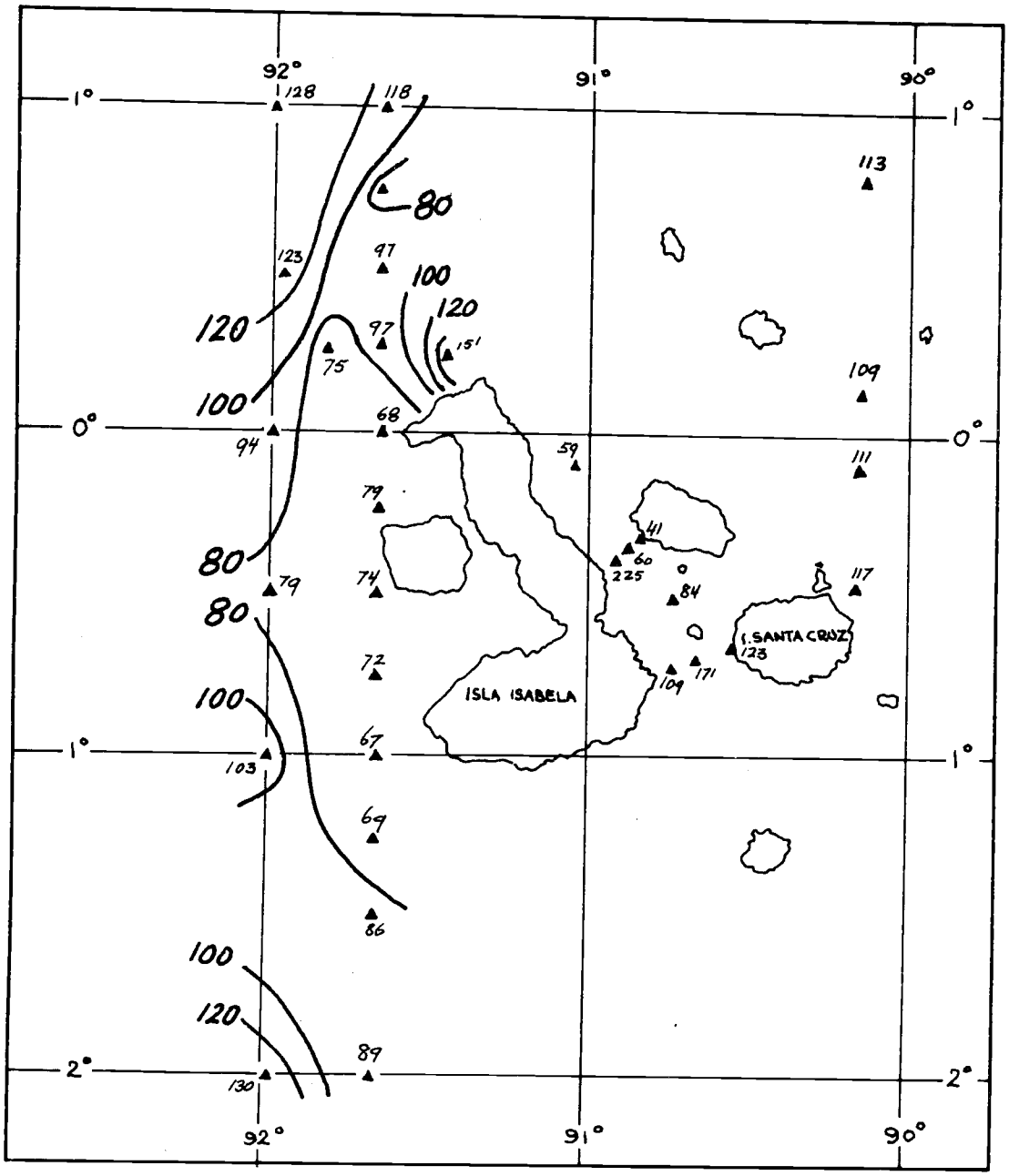

Figure 31. Light scattering at 45° $(\text{m-steradian})^{-1} \times 10^{-4}$ at 0 m depth.

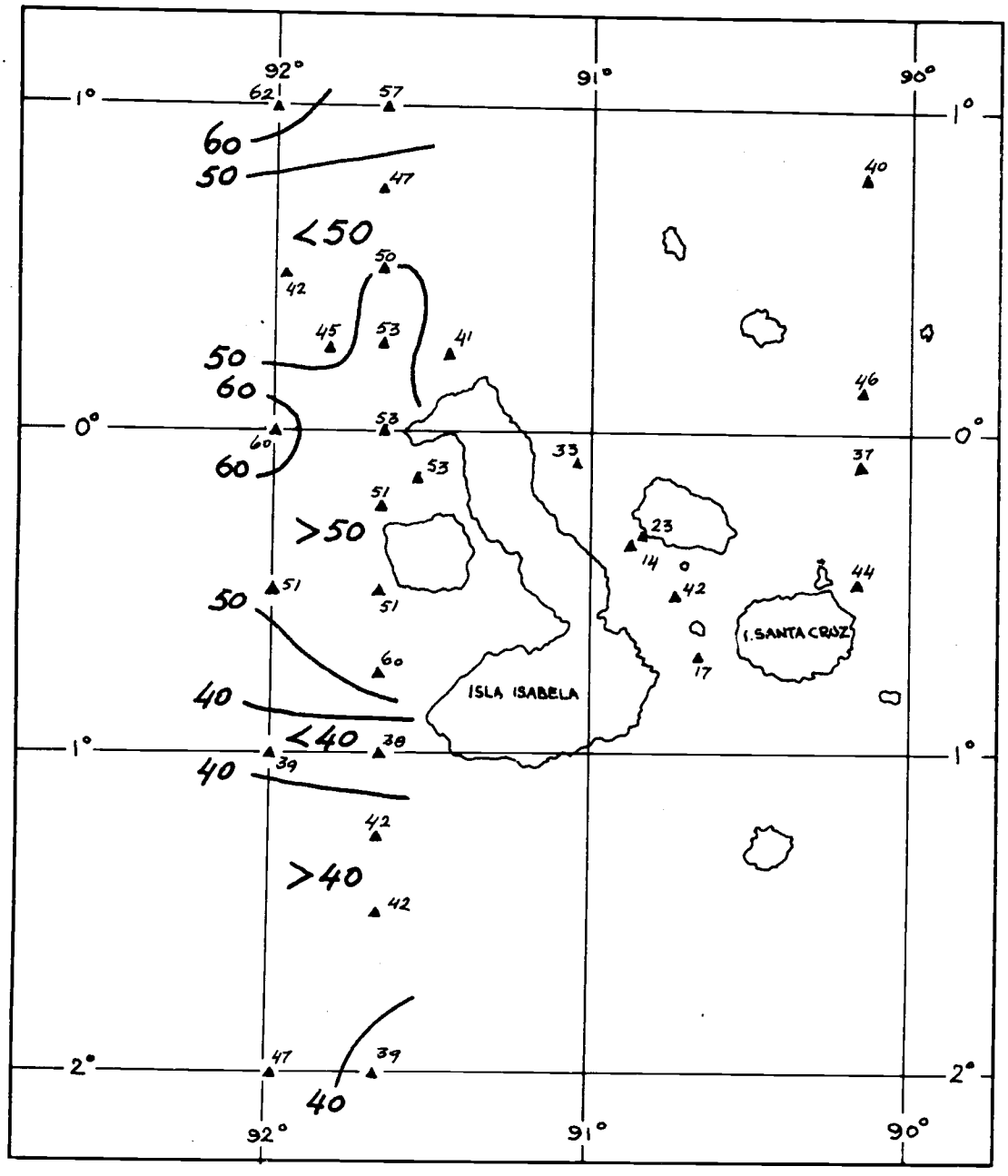

Figure 32. Light scattering at 45° $(\text{m-steradian})^{-1} \times 10^{-4}$ at 200 m depth.

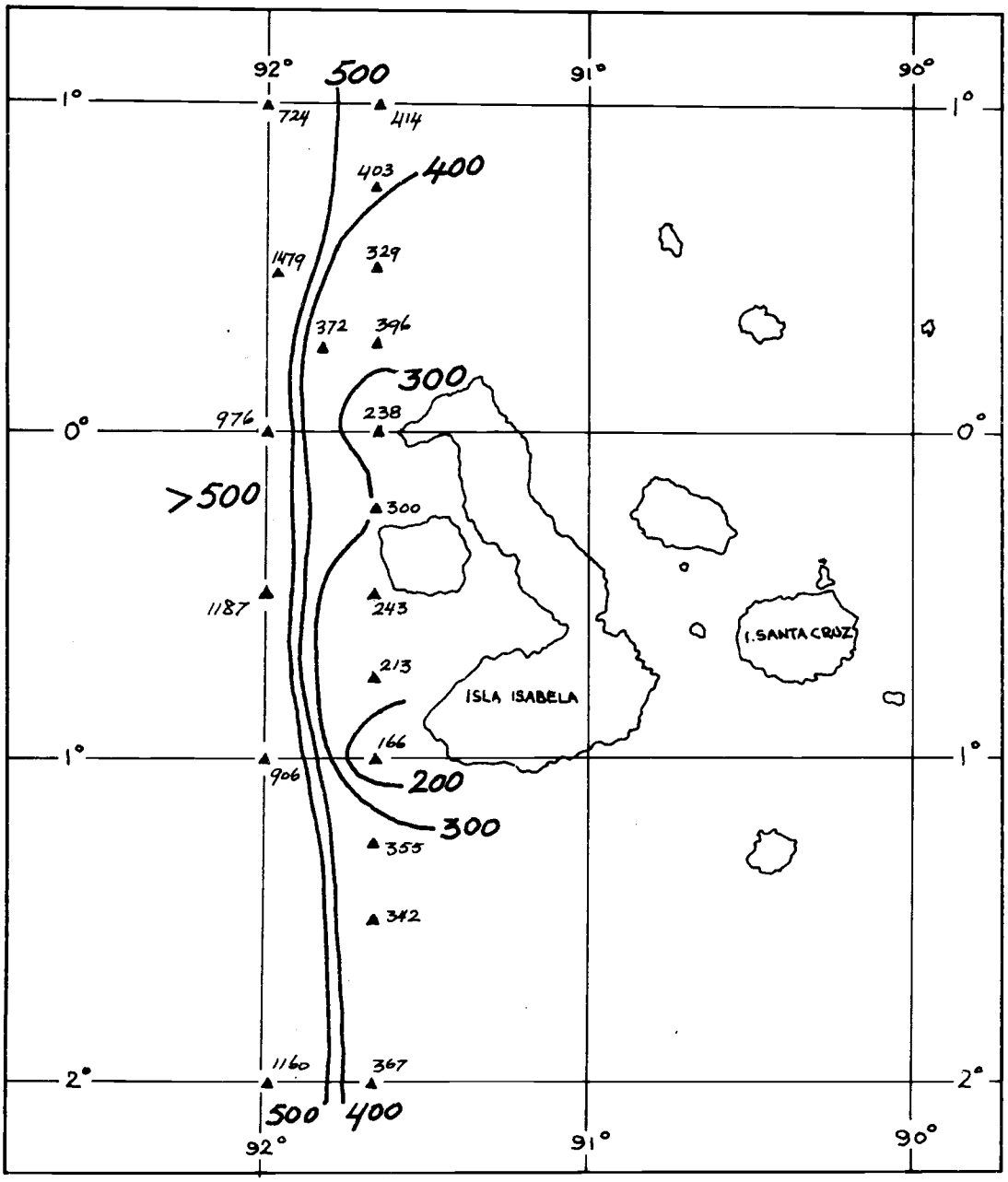

Figure 33. Total particle count per cc (greater than 2.2μ) at 0 m depth.

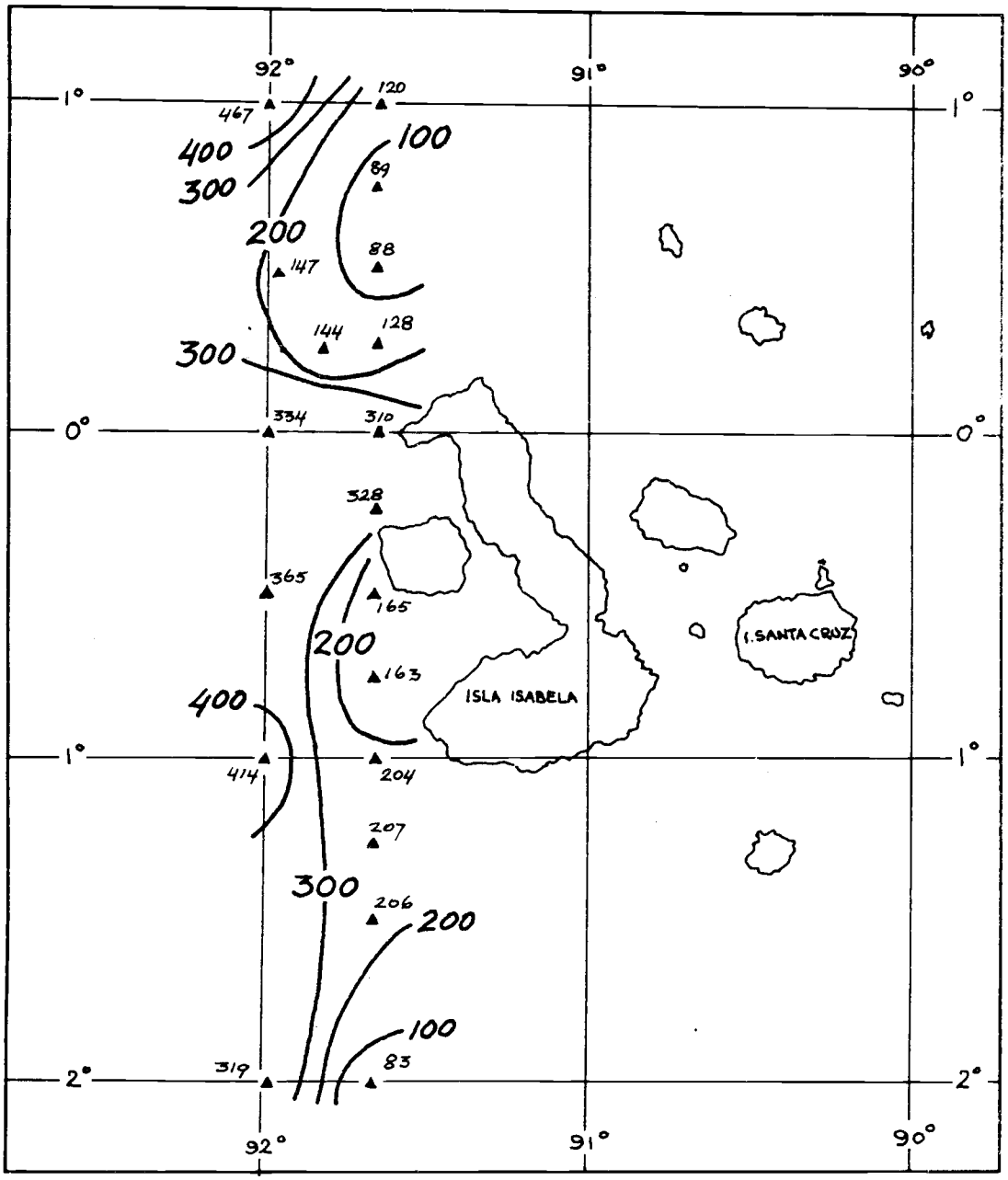

Figure 34. Total particle count per cc (greater than 2.2μ) at 100 m depth.

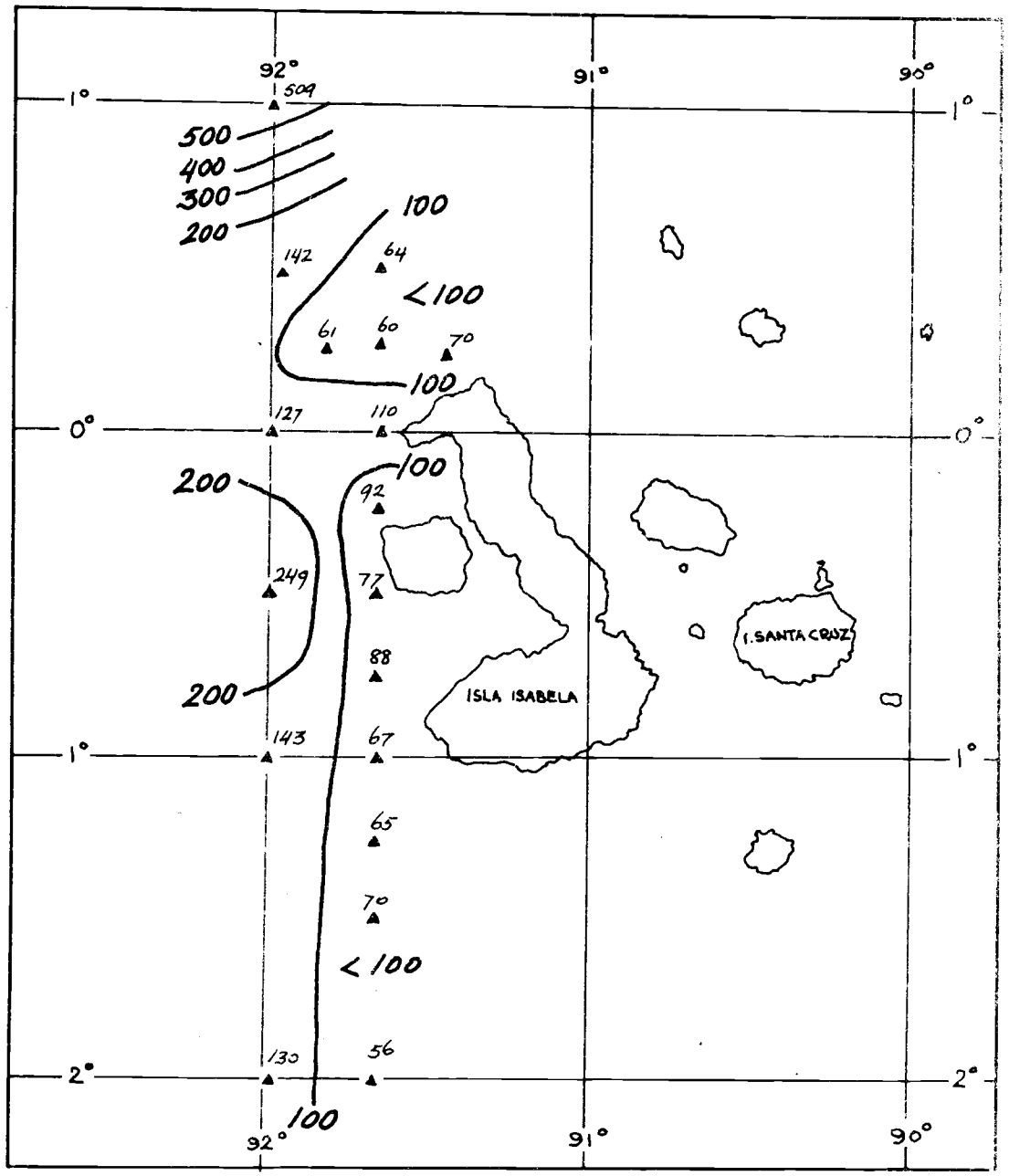

Figure 35. Total particle count per cc (greater than 2.2μ) at 200 m depth